

# Chapter 15

## Wing Scans: Analysis

*Terrance J. Gaetz*

In this chapter we discuss the analysis of the wing scan experiment at XRCF. The experiment was designed to map out the far wings of the Point Spread Function, or PSF, at angles  $\gtrsim 1$  mm (about  $20''$  away from the core) by using a series of pinhole scans across the PSF. Because of time constraints, only selected portions of the wings could be mapped in detail; a series of horizontal ( $Y$ ) or vertical ( $Z$ ) pinhole scans were sampled using pinhole diameters of 1, 4, 10, 20, and 35 mm. Quadrant shutters were used to isolate quadrants of individual mirror pairs; in order to provide illumination of the surface more nearly resembling on-orbit conditions, the HRMA was also pitched or yawed by the mean graze angle for the shell in question. The experiment, the reduction of the X-ray data, and the raytrace simulations of the pinhole measurements are discussed in more detail in Chapter 14.

The analysis of these data can provide information about two properties of the mirror: First, they allow the measurement of the RMS surface roughness of the mirrors, and a diagnosis of the amount of dust on the optics (if any). Second, by simply looking at the surface brightness as a function of off-axis angle, we can extrapolate the wings of the point spread function to discover how much of the effective area falls outside of the largest pinhole used in the Encircled Energy tests. This allows us to correct the measured effective areas at selected apertures for scattering beyond the largest aperture used.

In this chapter we discuss the analysis of X-ray wing scan data and the analysis of raytrace simulations of the wing scan experiment. The knowledge of the PSD based on the mirror metrology measurements is briefly discussed. The pinhole effective areas are combined to form surface brightness profiles for each of the sampled quadrants and energies, and the surface brightness profiles are in turn combined into PSD's in the form of “ $2W_1$ ” profiles. As a consistency check, the surface brightness profile is compared to that obtained by differentiating the effective area function in the one case which permits a relatively low-noise numerical derivative.

### 15.1 PSD based on HDOS metrology

Prior to X-ray testing at XRCF, knowledge of the microroughness of the HRMA optics depended on measurements of the HRMA mirror metrology performed at the Hughes Danbury Optical Systems, Inc. (HDOS) in Danbury, CT. Measurements were performed for each mirror after final polishing but before the mirror was shipped to OCLI for coating. The instruments used in the metrology were the CIDS (Circularity and Inner Diameter Station), the PMS (Precision Metrology

Station), and the MPMI or WYKO (Micro Phase Measuring Interferometer, a slightly modified WYKO Corporation instrument). The CIDS was used to determine circularity and the inner diameters of the HRMA shells. The PMS was used to measure along meridians. With these two instruments, HDOS essentially measured both the ‘hoops’ and ‘staves’ of each ‘barrel’ (optic), and thus mapped the entire surface. Finally, microroughness was sampled on each mirror using the WYKO.

The HDOS mirror metrology was processed by the AXAF Telescope Scientist into a low-frequency mirror map (based on PMS axial scan data and CIDS circularity data) and high frequency errors (based on WYKO measurements). These data were split into two pieces and processed into a mirror map for low-frequency errors (modeled in the raytrace using 2D splines periodic in one direction) and high frequency components (treated in the raytrace statistically as a scattering component).

The mirror map files represent a combination of PMS axial scan data and CIDS circularity data. Each of these files had solid body translations and rotations removed and was divided into two complementary maps by passing the data through a filter; the low pass portions were combined with the modeled distortions induced by the mirror supports (1G and epoxy-induced distortions), fit with 2D spline functions, and used deterministically in the ray-tracing. The high frequency portions were combined with the WYKO data and treated statistically in the raytraces. The standard HDOS filter was used for the separation; the parameters were such that the transition between low and high frequency pass bands occurred from 0.02 to 0.03  $\text{mm}^{-1}$ .

The WYKO data at each magnification ( $\times 1.5$ ,  $\times 10$ , and  $\times 40$ ) were combined into mean PSD files, and these files were processed with the program `foldw1` (which is similar to the HDOS program `eegraz`) to calculate scattering distributions. The calculation was based on the Kirchoff theory of scattering Beckmann and Spizzichino (1963). The PSD files do not agree perfectly in the overlap regions, so a linear weighting was used in the overlap regions such that the weight given to the lower frequency file would decrease from 1.0 to 0.0 while the weight given to the high frequency file would increase from 0.0 to 1.0. The frequency intervals are, in units of  $\text{mm}^{-1}$ , 0.000 to 0.226, 0.226 to 0.5, 0.5 to 1.5, 1.5 to 2.0, 2.0 to 5.0, 5.0 to 10.0, and 10.0 to 1000.0.

Because the mirror surface roughness is worse near the end of each mirror, the PSDs were calculated for a set of axial zones (ranging from 5 to 11 zones) for each optic, with a center zone covering about 80% of the mirror surface and end zones covering the rest.

### 15.2 Surface Brightness Profiles

Once the wing scan pinhole effective areas are obtained (see Chapter 14), the next level of processing is to stitch together the pinhole effective areas into surface brightness profiles for a given shell, quadrant, and energy. The pinhole effective area is converted to a surface brightness,  $\psi$ , normalized to the effective area within a 35 mm diameter pinhole on-axis and scaled by a factor of  $2 \times 88/360$  to account for the fact that the experiment used a single quadrant at a time. The effective area measured within a 35 mm diameter on-axis pinhole will be denoted  $A_{eff}^{tot}$ ; in the raytrace simulation,  $A_{eff}^{tot}$  was evaluated from an on-axis raytrace with a 35 mm diameter pinhole at the appropriate axial location.

The *scaled* on-axis 35 mm effective area is  $a_{eff}^{tot}$ , where

$$a_{eff}^{tot} = 2 \times \frac{88}{360} A_{eff}^{tot}. \quad (15.1)$$

The factor 88/360 arises because each “quadrant” is really  $88^\circ$  (because of the overlap of adjacent closed quadrants). The factor of 2 comes about because scattering is predominantly in-plane so

that the scattered flux at a given off-axis location comes primarily from two opposing portions of the mirror; having only one shutter open should provide about half the flux, provided that the pinhole doesn't actually contain the core of the PSF. This factor should be verified by raytrace experiments; however, obtaining sufficiently small errors would require significantly longer raytraces than performed thus far.

The surface brightness is estimated as

$$\psi = w \times \frac{A_{eff}}{a_{eff}^{tot}} \times \frac{4F_{fc}^2}{\pi d^2}, \quad (15.2)$$

where  $w$  is a wing correction factor (see below),  $F_{fc}$  is the telescope finite conjugate focal length (taken to be 10.252500 m),  $A_{eff}$  is the measured effective area through the off-centered aperture of diameter  $d$  obtained as part of the wingscan test, and  $a_{eff}^{tot}$  the rescaled on-axis 35 mm effective area with all four quadrants exposed (see Eq. Eq. 15.1).

The surface brightness,  $\psi$ , should really be normalized to  $\int_{2\pi} \psi d\Omega = 1$ ; by normalizing to a 35 mm diameter pinhole we neglect the flux which falls outside the pinhole. This is at most a 4% (**TBR**) effect for the XRCF data (and usually smaller), and an even smaller effect in the case of the current raytrace simulations.

In evaluating the surface brightness, the pinhole effective areas need to be corrected for the fact that the pinhole has a finite diameter and samples the wings of a PSF which is falling steeply with radius. Consequently, the flux can vary strongly with position within the pinhole; in some cases the pinhole diameter is as large as the pinhole off-axis distance, so the effect can be significant. The analysis currently assumes that the brightness falls as a power law across the width of a pinhole, *i.e.*

$$\psi = \psi_0 \theta^{-\gamma}, \quad (15.3)$$

with  $\gamma$  constant across the pinhole. The pinhole correction then becomes the factor

$$w \approx \frac{1}{{}_2F_1\left(\frac{\gamma}{2}, \frac{\gamma}{2}, 2; \frac{a^2}{r^2}\right)} \quad (15.4)$$

where  $a$  is the pinhole radius,  $r$  is the off-axis distance, and  ${}_2F_1$  is a hypergeometric function.

The value of  $\gamma$  was obtained by using the local logarithmic derivative of the fit function (Eq. 15.5) at the location of the pinhole center (see below).

The surface brightness data are fit with functions of the form

$$\psi(R) = aR^{-b}e^{-R/c} \quad (15.5)$$

where  $R$  is the distance (in mm) in the  $Y-Z$  plane of the pinhole center from the finite conjugate focus;  $R$  is related to off-axis angle  $\theta$  by

$$\theta \approx R/F_{fc}, \quad (15.6)$$

where  $F_{fc}$  is the distance from the HRMA node to the finite conjugate focus.

It is necessary to obtain the wing correction iteratively. We begin by assuming  $\gamma = 2$ , compute surface brightnesses, and fit the surface brightness to an exponentially truncated power law (Eq. Eq. 15.5). In the case of  $\gamma = 2$ , the hypergeometric function reduces to

$${}_2F_1\left(1, 1, 2; \frac{a^2}{r^2}\right) = -\frac{\ln(1-z)}{z} \quad (15.7)$$

We take the logarithmic derivative of this function to obtain the local power-law index  $\gamma$  at each data point  $\theta$ , recompute the wing correction using the hypergeometric function, and iterate until

$$\Delta \equiv \sum_{\text{ap pos}} \left( \frac{w_{old} - w_{new}}{w_{old}} \right)^2 \leq 0.01 \quad (15.8)$$

or 5 iterations, whichever is smaller. In the case of the data from raytrace simulations, 5 iterations were always performed. The raytrace data are not fit well by this form; the raytrace surface brightness profiles contain much structure from the underlying assumed surface PSD, so an unconstrained fit can be a poor approximation to the overall data set. In particular, in attempting to reduce large  $\chi^2$  contributions from large curvature portions at small radius, the unconstrained fit may introduce a relatively small value for the exponential cutoff scale length so that the fit function cuts off well before the data. It was decided against attempting to fit more realistic functions to the raytrace data; ultimately we need to compare against the fits to the XRCF data, and the sparseness of the XRCF data set would not support a functional form with even more free parameters. In order to reduce the problems with the exponential cutoff scale, the exponential scale length parameter for the raytrace fits was typically limited to a range of values (typically 20 - 10000 mm); the lower limit was a value chosen (by trial and error) to reproduce the overall shape of the curve at large radii. This worked in some cases (*e.g.*, Figure 15.3) but not very well in other cases (*e.g.*, Figure 15.6). For the present we use the same limits for the exponential cutoff, but future analyses should consider applying different limit ranges on a case by case basis. The XRCF data sets were much sparser and this seems to have been less of a problem; see the shell 6 fits, however.

As noted in §14.2.3, vignetting resulting from the adjacent closed quadrant shutters can be significant. Because of this, separate fits were made for scattering towards the optic (*i.e.*, towards larger radii at the focal plane) and away from the optic (towards smaller radii at the focal plane) for each shell, quadrant, and energy. In the case of the raytrace data, the data points subject to vignetting were removed from the plots and the fits; the adopted cutoffs are listed in Table 15.1.

Table 15.1: Wing scan shutter vignetting cutoffs

| Shell | Towards optic<br>(mm) | Away from optic<br>(mm) |
|-------|-----------------------|-------------------------|
| 1     | 70                    | 500                     |
| 3     | 500                   | 30                      |
| 4     | 50                    | 500                     |
| 6     | 500                   | 500                     |

The XRCF data are compared to the raytrace simulations in the following tables and figures. In the following, §15.2.1 presents the surface brightness data for the shell 1 single quadrant wing scans in the order: quadrant, energy. Similarly, §15.2.2, §15.2.3, and §15.2.4 present the single quadrant wing scan data for shells 3, 4, and 6, respectively. Finally, §15.2.5 presents the surface brightness data for the shell 4 and shell 6 double-quadrant wing scans. Tables 15.2 to 15.8 present the parameters for the fits to the XRCF data points and to the raytrace data. The fits are also used to evaluate the fractional excess effective area falling outside the largest (35 mm diameter pinhole); this is at most ~4% (**TBR**) in the case of the XRCF data and at most ~2% (**TBR**) for the raytrace simulations. Note that in most cases the fractional excess effective area is considerably smaller than the worst case.

The agreement between the XRCF data and the raytrace simulations seems to be reasonably good for the smallest pinholes. The data for the 1S scan at Al-K $\alpha$  seem to show considerably more

scattering in the direction away from the optic than towards the optic. This is also particularly noticeable in all four quadrants for the the Al-K $\alpha$  scans shell 3, and for quadrant 4S. This effect seems to be less prominent in the other quadrant/shell/energy combinations. The reason for – and significance of – this effect is not well understood at present.

### 15.2.1 Shell 1 scans

Table 15.2: Surface brightness fits and fractional excess effective area beyond the 35 mm pinhole. (Raytrace simulations and XRCF data, Shell 1)

| Type | Quad | Line | Dir | a          | b     | c         | fractional extra area |
|------|------|------|-----|------------|-------|-----------|-----------------------|
| sim  | 1T   | Al   | in  | 177526.000 | 2.447 | 145.081   | 0.001618              |
| sim  | 1T   | Al   | out | 100141.600 | 2.039 | 32.969    | 0.001009              |
| sim  | 1N   | Al   | in  | 188074.000 | 2.414 | 100.808   | 0.001539              |
| sim  | 1N   | Al   | out | 140240.000 | 2.145 | 36.331    | 0.001089              |
| sim  | 1B   | Al   | in  | 229218.000 | 2.540 | 354.215   | 0.002089              |
| sim  | 1B   | Al   | out | 142126.000 | 2.074 | 33.888    | 0.001309              |
| sim  | 1S   | Al   | in  | 239490.000 | 2.442 | 68.289    | 0.001245              |
| sim  | 1S   | Al   | out | 135748.000 | 2.063 | 32.608    | 0.001222              |
| sim  | 1T   | Ti   | in  | 638360.000 | 2.083 | 22.409    | 0.002511              |
| sim  | 1T   | Ti   | out | 491692.000 | 1.982 | 20.000    | 0.002182              |
| sim  | 1N   | Ti   | in  | 651161.000 | 2.069 | 22.748    | 0.002793              |
| sim  | 1N   | Ti   | out | 544555.000 | 1.992 | 20.000    | 0.002326              |
| sim  | 1B   | Ti   | in  | 715540.000 | 2.108 | 23.324    | 0.002788              |
| sim  | 1B   | Ti   | out | 514720.000 | 1.923 | 20.000    | 0.002870              |
| sim  | 1S   | Ti   | in  | 709070.000 | 2.053 | 20.000    | 0.002390              |
| sim  | 1S   | Ti   | out | 495692.000 | 1.923 | 20.000    | 0.002761              |
| xrcf | 1T   | Al   | in  | 174886.000 | 2.202 | 374.817   | 0.007554              |
| xrcf | 1T   | Al   | out | 161181.000 | 2.061 | 188.814   | 0.009362              |
| xrcf | 1N   | Al   | in  | 146541.000 | 1.933 | 48.627    | 0.004132              |
| xrcf | 1N   | Al   | out | 151190.000 | 1.965 | 88.460    | 0.007418              |
| xrcf | 1B   | Al   | in  | 135389.000 | 2.271 | 10000.000 | 0.008287              |
| xrcf | 1B   | Al   | out | 123336.000 | 1.947 | 76.618    | 0.005657              |
| xrcf | 1S   | Al   | in  | 90294.800  | 1.837 | 47.734    | 0.003680              |
| xrcf | 1S   | Al   | out | 209820.000 | 2.214 | 10000.000 | 0.017700              |
| xrcf | 1T   | Ti   | in  | 588435.000 | 1.640 | 32.729    | 0.028977              |
| xrcf | 1T   | Ti   | out | 650222.000 | 1.713 | 29.945    | 0.020186              |
| xrcf | 1N   | Ti   | in  | 654973.000 | 1.624 | 26.366    | 0.022367              |
| xrcf | 1N   | Ti   | out | 741870.000 | 1.851 | 39.998    | 0.021932              |
| xrcf | 1B   | Ti   | in  | 564424.000 | 1.803 | 63.980    | 0.038846              |
| xrcf | 1B   | Ti   | out | 477645.000 | 1.605 | 27.270    | 0.018891              |
| xrcf | 1S   | Ti   | in  | 518891.000 | 1.634 | 30.179    | 0.022434              |
| xrcf | 1S   | Ti   | out | 686177.000 | 1.759 | 32.517    | 0.020691              |

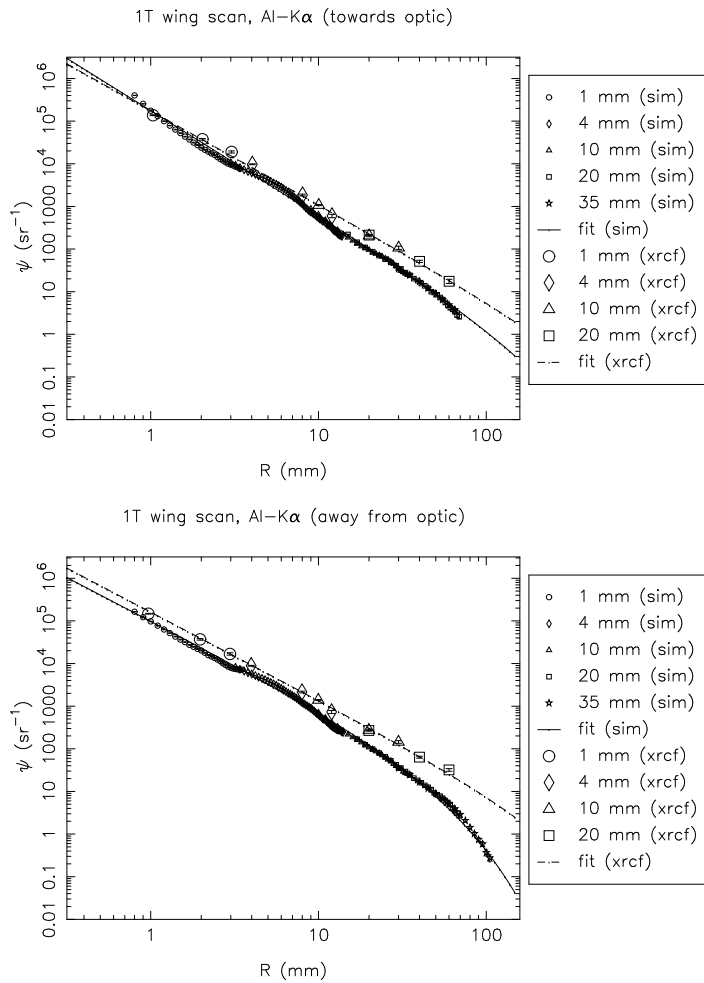


Figure 15.1: Shell 1T: Al-K $\alpha$  surface brightness, towards and away from the optic

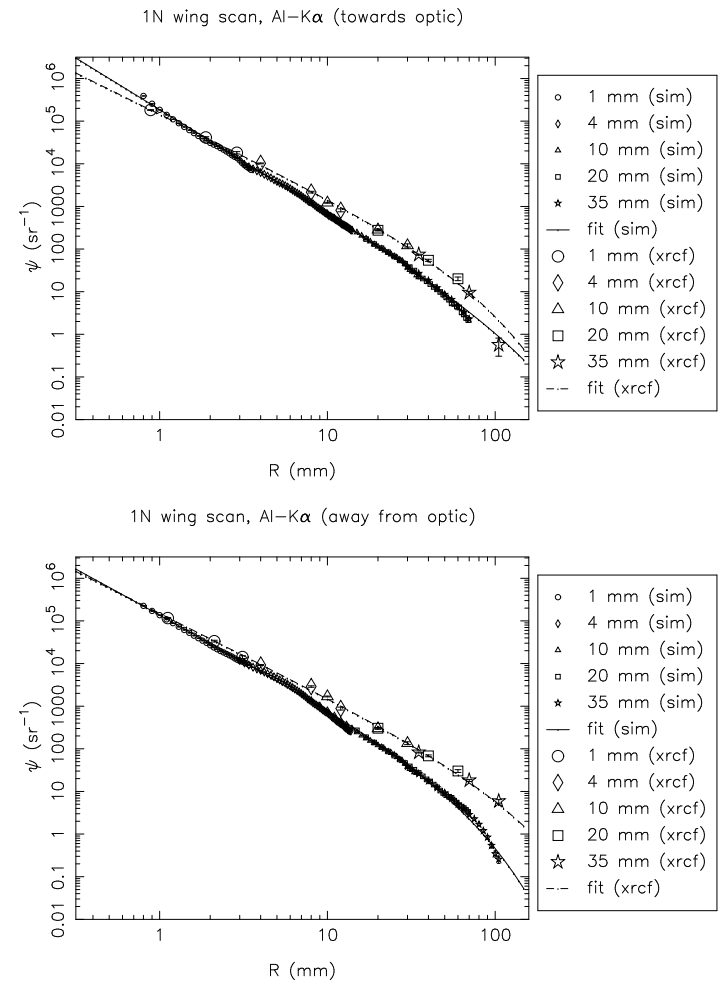


Figure 15.2: Shell 1N: Al-K $\alpha$  surface brightness, towards and away from the optic

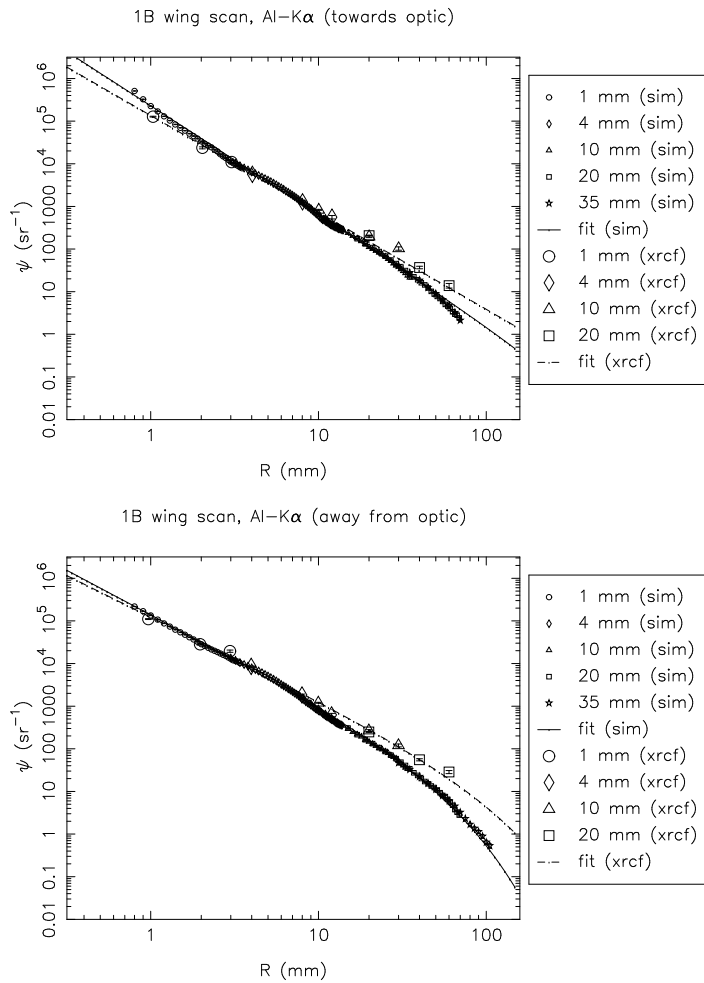


Figure 15.3: Shell 1B: Al-K $\alpha$  surface brightness, towards and away from the optic

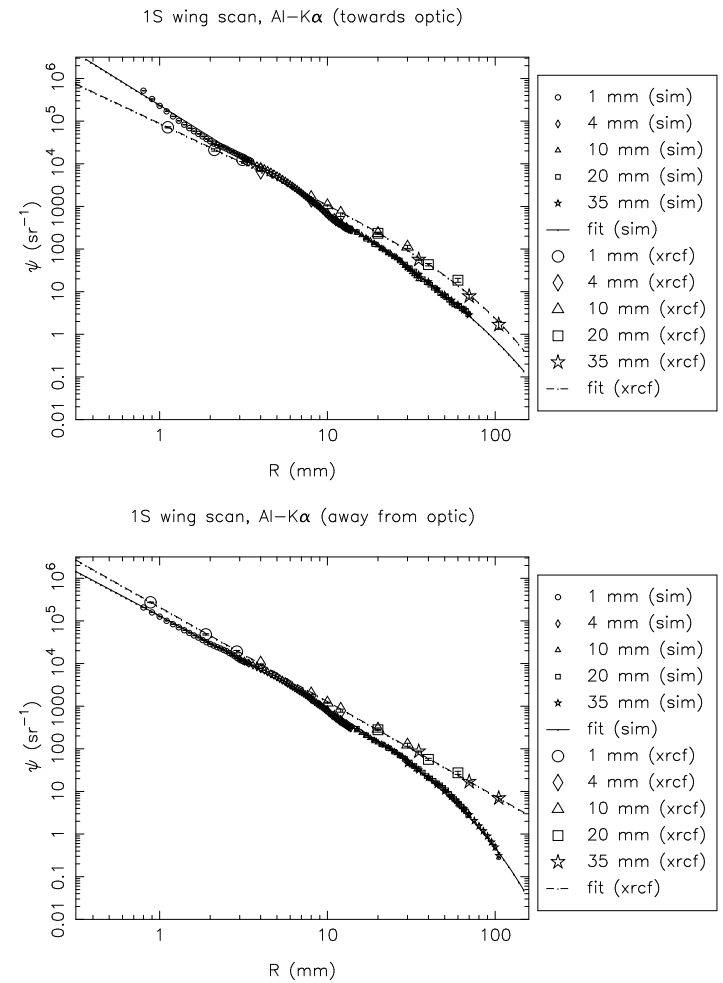


Figure 15.4: Shell 1S: Al-K $\alpha$  surface brightness, towards and away from the optic

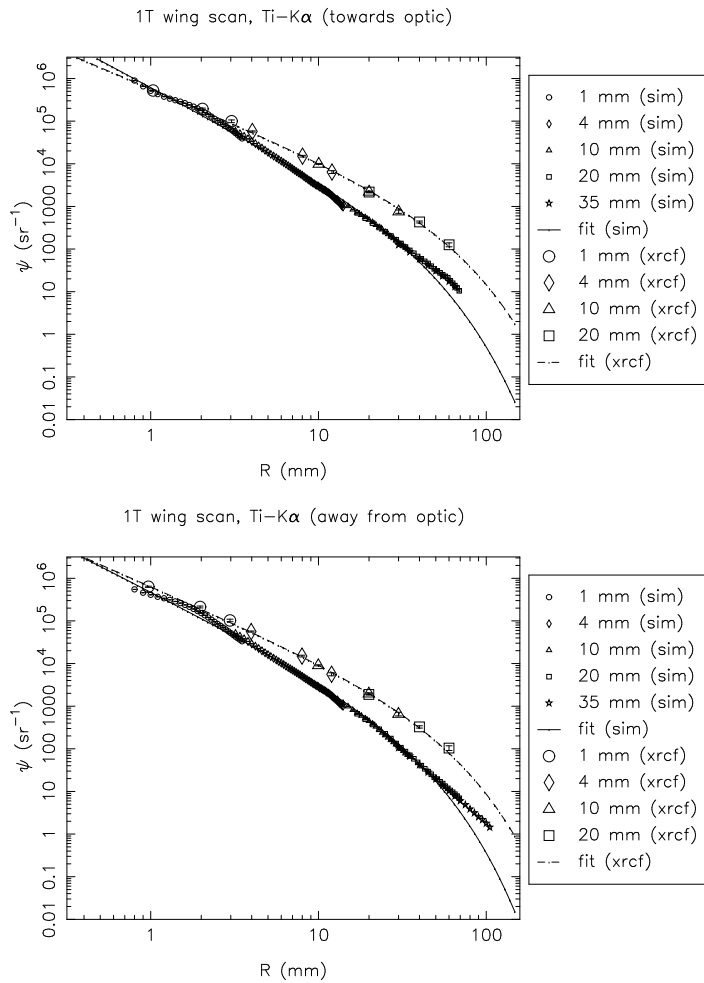


Figure 15.5: Shell 1T: Ti-K $\alpha$  surface brightness, towards and away from the optic

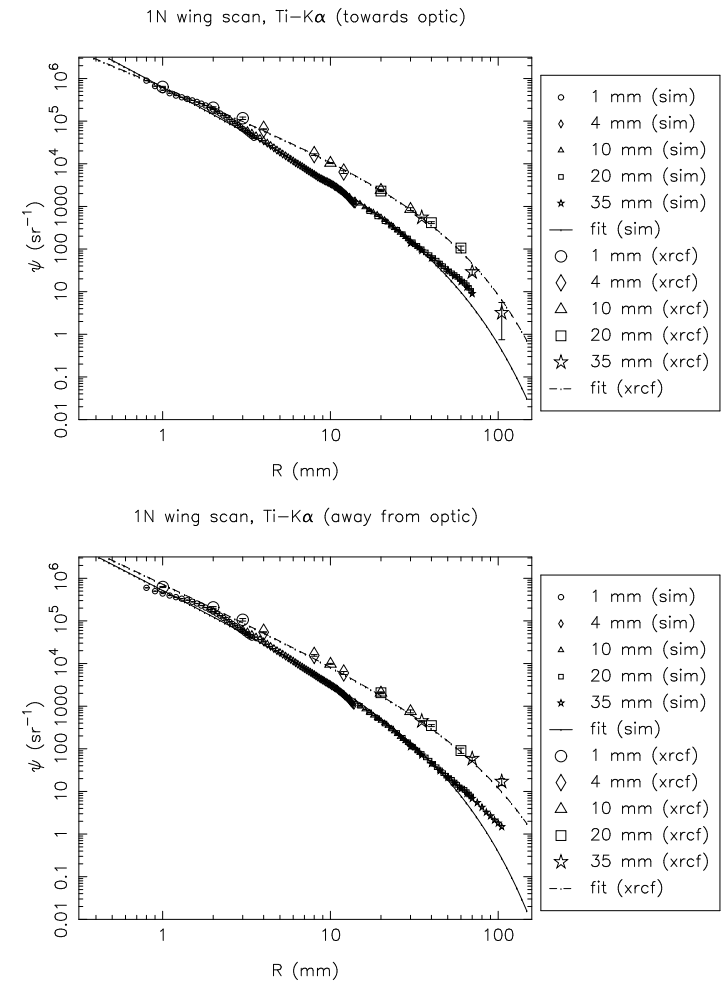


Figure 15.6: Shell 1N: Ti-K $\alpha$  surface brightness, towards and away from the optic

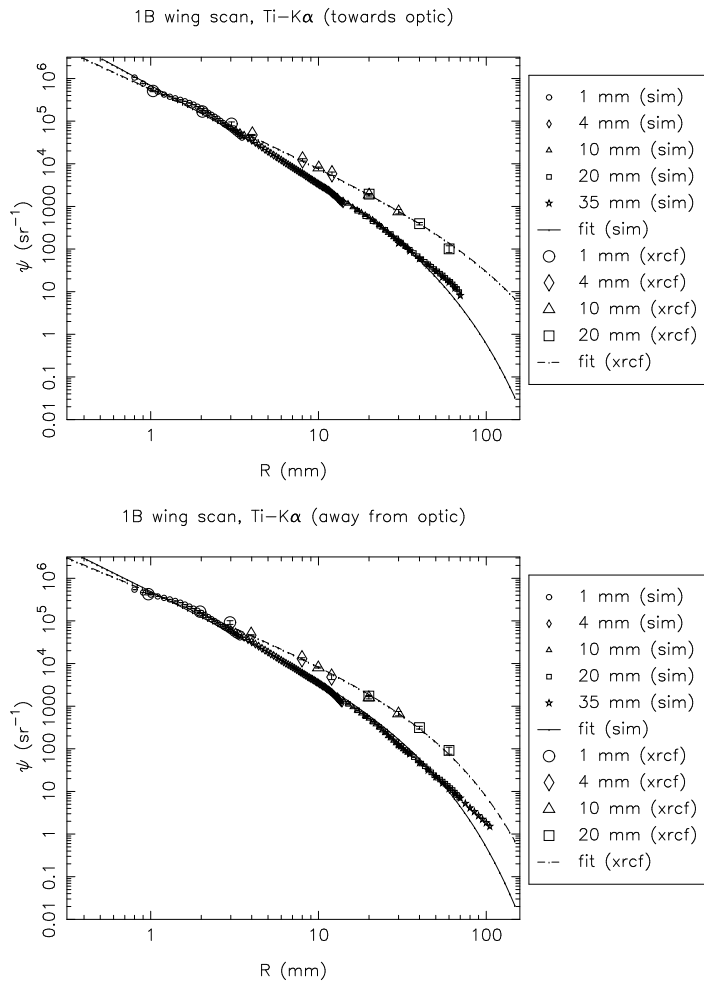


Figure 15.7: Shell 1B: Ti-K $\alpha$  surface brightness, towards and away from the optic

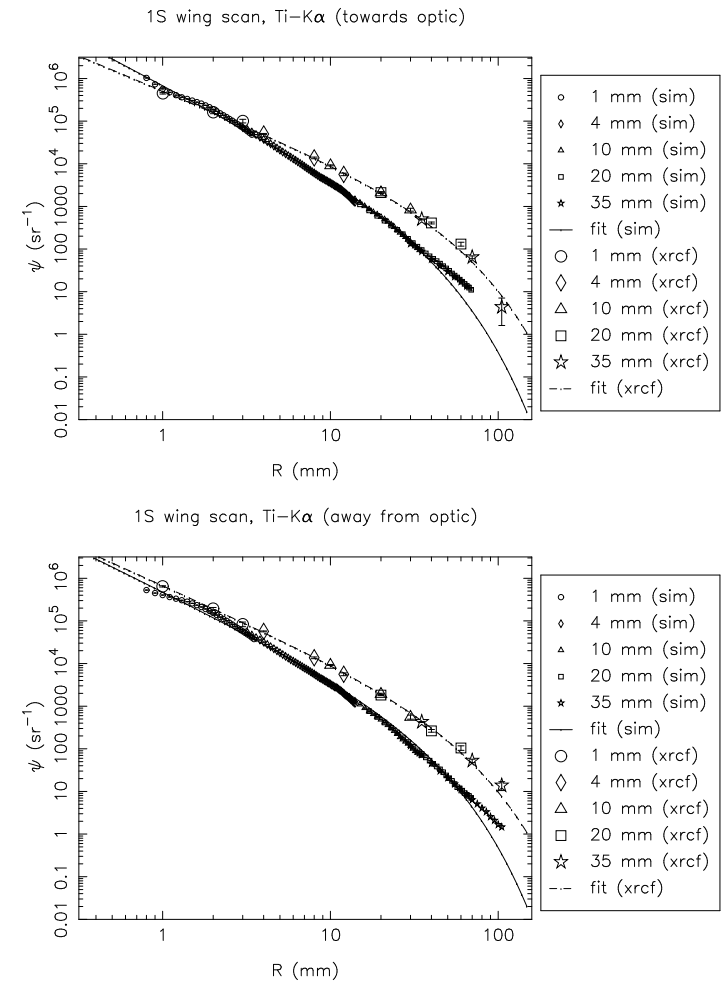


Figure 15.8: Shell 1S: Ti-K $\alpha$  surface brightness, towards and away from the optic

## 15.2.2 Shell 3 scans

Table 15.3: Surface brightness fits and fractional excess effective area beyond the 35 mm pinhole. (Raytrace simulations, Shell 3)

| Type | Quad | Line | Dir | a          | b     | c         | fractional extra area |
|------|------|------|-----|------------|-------|-----------|-----------------------|
| sim  | 3T   | Al   | in  | 33670.200  | 2.630 | 10000.000 | 0.000318              |
| sim  | 3T   | Al   | out | 18158.600  | 2.123 | 70.000    | 0.000361              |
| sim  | 3N   | Al   | in  | 43456.300  | 2.810 | 10000.000 | 0.000173              |
| sim  | 3N   | Al   | out | 21399.700  | 2.290 | 164.721   | 0.000415              |
| sim  | 3B   | Al   | in  | 33533.400  | 2.612 | 10000.000 | 0.000345              |
| sim  | 3B   | Al   | out | 20187.700  | 2.193 | 70.000    | 0.000301              |
| sim  | 3S   | Al   | in  | 33600.500  | 2.621 | 10000.000 | 0.000332              |
| sim  | 3S   | Al   | out | 15612.400  | 2.026 | 70.000    | 0.000466              |
| sim  | 3S   | Ti   | in  | 186937.000 | 2.570 | 70.000    | 0.000591              |
| sim  | 3S   | Ti   | out | 124877.000 | 2.335 | 70.000    | 0.001034              |
| sim  | 3S   | Cr   | in  | 246429.000 | 2.579 | 70.000    | 0.000749              |
| sim  | 3S   | Cr   | out | 176035.000 | 2.408 | 70.000    | 0.001081              |
| sim  | 3T   | Fe   | in  | 349548.000 | 2.561 | 85.408    | 0.001361              |
| sim  | 3T   | Fe   | out | 270453.000 | 2.539 | 70.000    | 0.000968              |
| sim  | 3B   | Fe   | in  | 353953.000 | 2.603 | 117.001   | 0.001461              |
| sim  | 3B   | Fe   | out | 254630.000 | 2.510 | 70.000    | 0.001028              |
| sim  | 3N   | Fe   | in  | 377381.000 | 2.626 | 148.135   | 0.001626              |
| sim  | 3N   | Fe   | out | 293686.000 | 2.532 | 70.000    | 0.001081              |
| sim  | 3S   | Fe   | in  | 362943.000 | 2.575 | 70.000    | 0.001125              |
| sim  | 3S   | Fe   | out | 226964.000 | 2.524 | 70.000    | 0.000866              |

Table 15.4: Surface brightness fits and fractional excess effective area beyond the 35 mm pinhole. (XRCF data, Shell 3)

| Type | Quad | Line | Dir | a          | b     | c         | fractional extra area |
|------|------|------|-----|------------|-------|-----------|-----------------------|
| xrcf | 3T   | Al   | in  | 42694.600  | 2.545 | 10000.000 | 0.000615              |
| xrcf | 3T   | Al   | out | 139570.000 | 2.700 | 10000.000 | 0.000937              |
| xrcf | 3N   | Al   | in  | 25452.400  | 1.980 | 42.306    | 0.000486              |
| xrcf | 3N   | Al   | out | 123052.000 | 2.509 | 71.304    | 0.000507              |
| xrcf | 3B   | Al   | in  | 18670.600  | 1.721 | 20.099    | 0.000231              |
| xrcf | 3B   | Al   | out | 55033.600  | 2.205 | 77.562    | 0.000863              |
| xrcf | 3S   | Al   | in  | 16015.000  | 1.783 | 30.189    | 0.000382              |
| xrcf | 3S   | Al   | out | 62529.500  | 2.125 | 25.698    | 0.000281              |
| xrcf | 3S   | Ti   | in  | 278681.000 | 2.231 | 122.589   | 0.005740              |
| xrcf | 3S   | Ti   | out | 195982.000 | 1.925 | 31.936    | 0.002944              |
| xrcf | 3S   | Cr   | in  | 260346.000 | 2.095 | 65.196    | 0.005399              |
| xrcf | 3S   | Cr   | out | 310305.000 | 2.009 | 25.242    | 0.002115              |
| xrcf | 3T   | Fe   | in  | 560465.000 | 2.253 | 459.946   | 0.020630              |
| xrcf | 3T   | Fe   | out | 736608.000 | 2.304 | 33.052    | 0.002609              |
| xrcf | 3B   | Fe   | in  | 568188.000 | 2.304 | 232.852   | 0.012476              |
| xrcf | 3B   | Fe   | out | 484538.000 | 2.107 | 29.203    | 0.003001              |
| xrcf | 3N   | Fe   | in  | 422225.000 | 2.114 | 59.864    | 0.007351              |
| xrcf | 3N   | Fe   | out | 563223.000 | 2.168 | 21.617    | 0.001465              |
| xrcf | 3S   | Fe   | in  | 503919.000 | 2.113 | 58.980    | 0.008658              |
| xrcf | 3S   | Fe   | out | 428822.000 | 2.027 | 20.240    | 0.001646              |

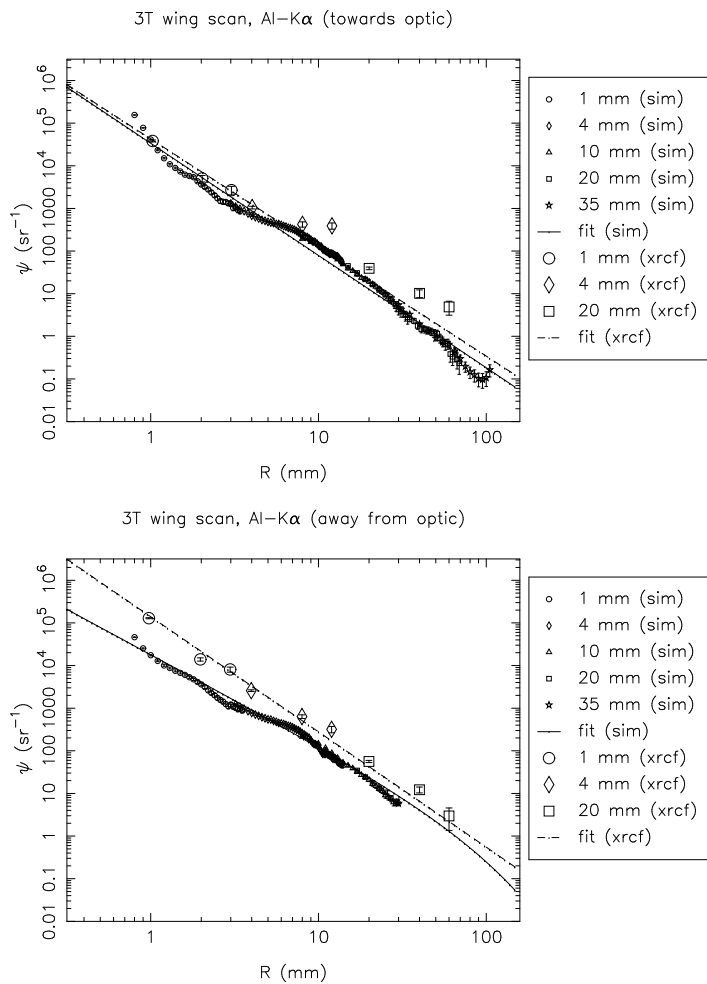


Figure 15.9: Shell 3T: Al-K $\alpha$  surface brightness, towards and away from the optic

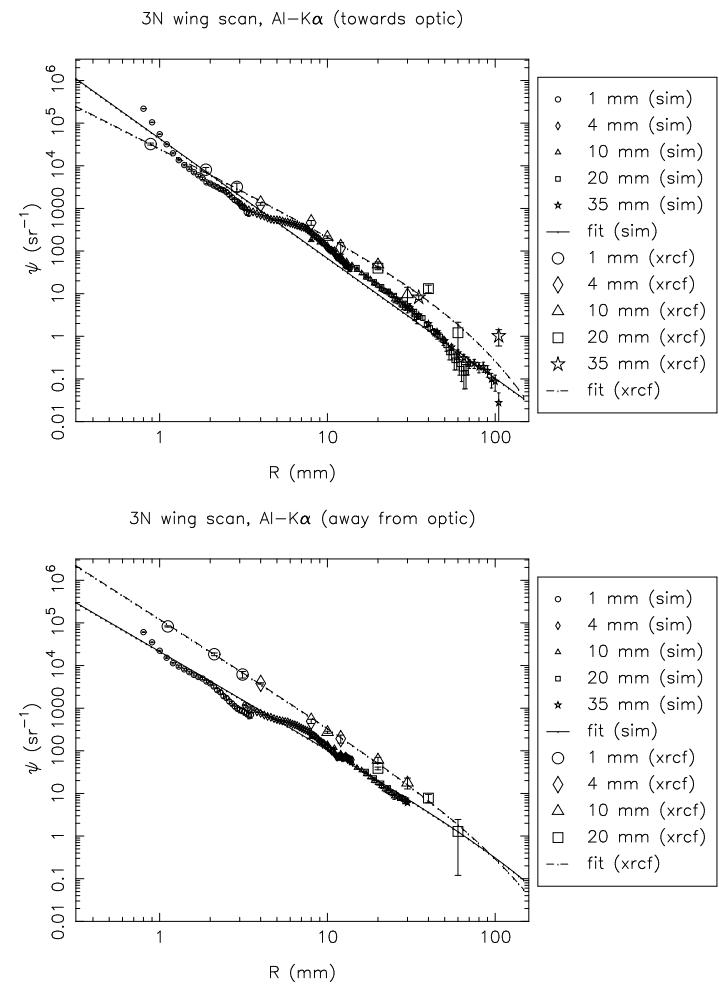
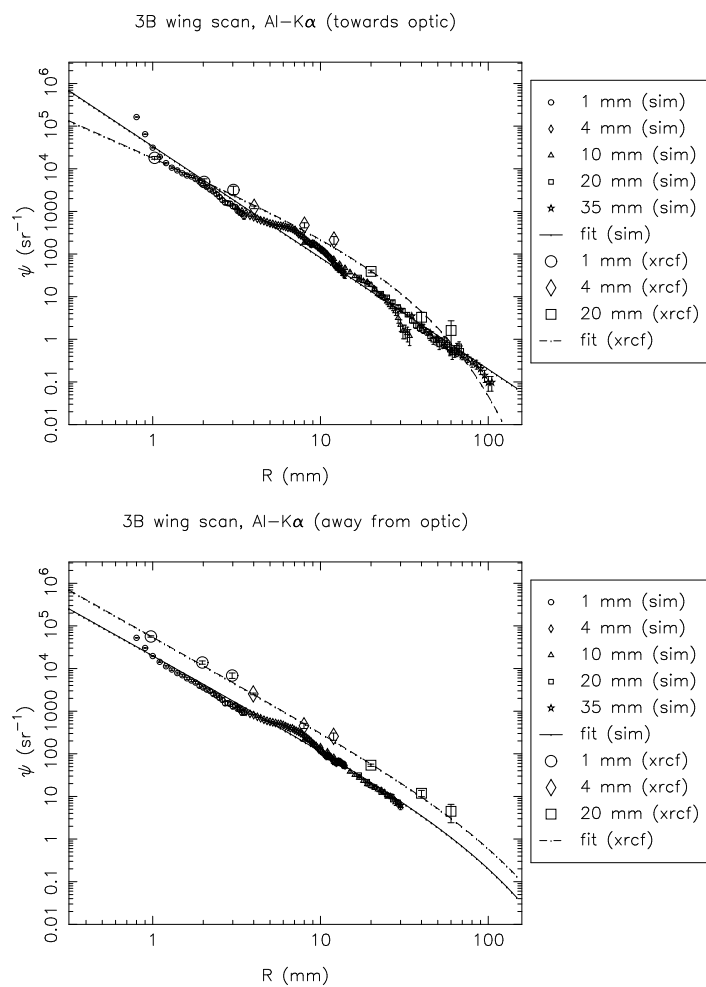
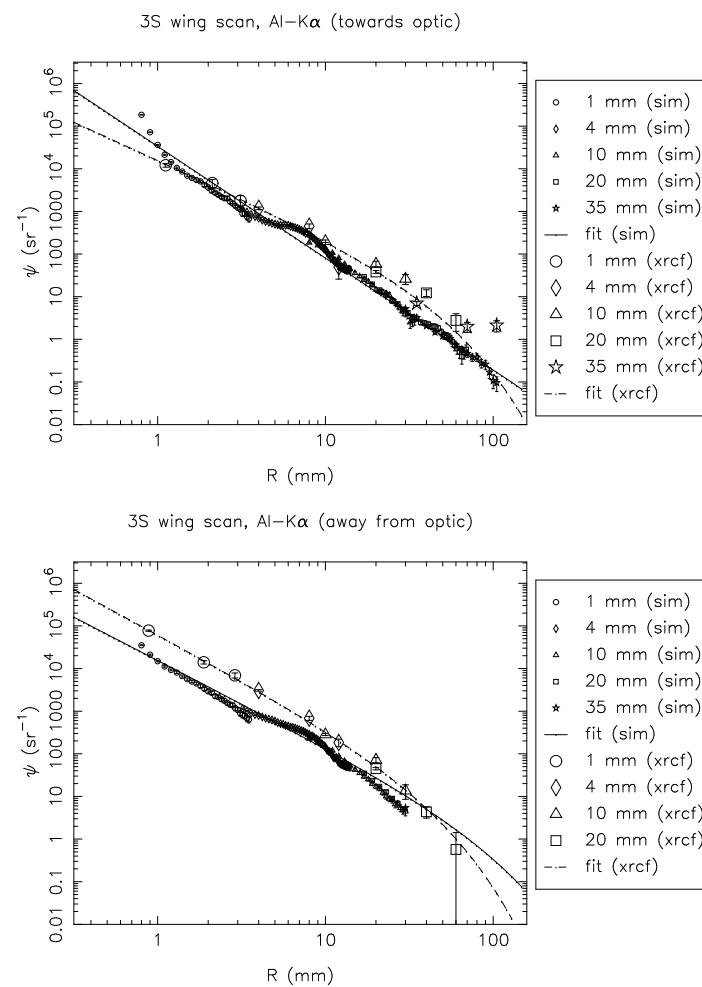


Figure 15.10: Shell 3N: Al-K $\alpha$  surface brightness, towards and away from the optic

Figure 15.11: Shell 3B: Al-K $\alpha$  surface brightness, towards and away from the opticFigure 15.12: Shell 3S: Al-K $\alpha$  surface brightness, towards and away from the optic

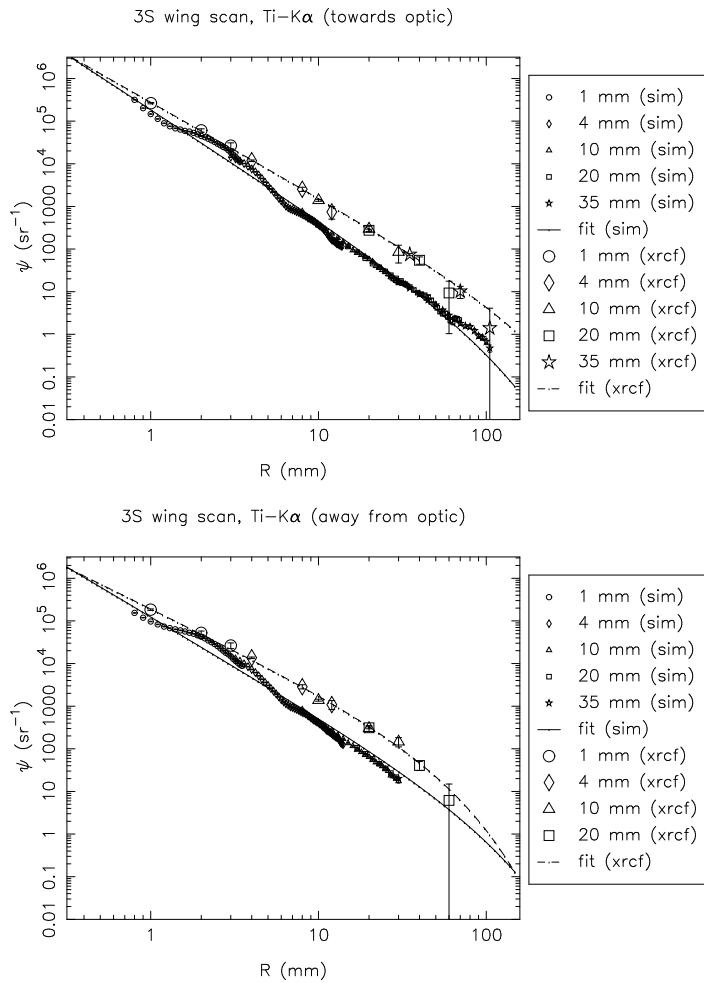


Figure 15.13: Shell 3S: Ti-K $\alpha$  surface brightness, towards and away from the optic

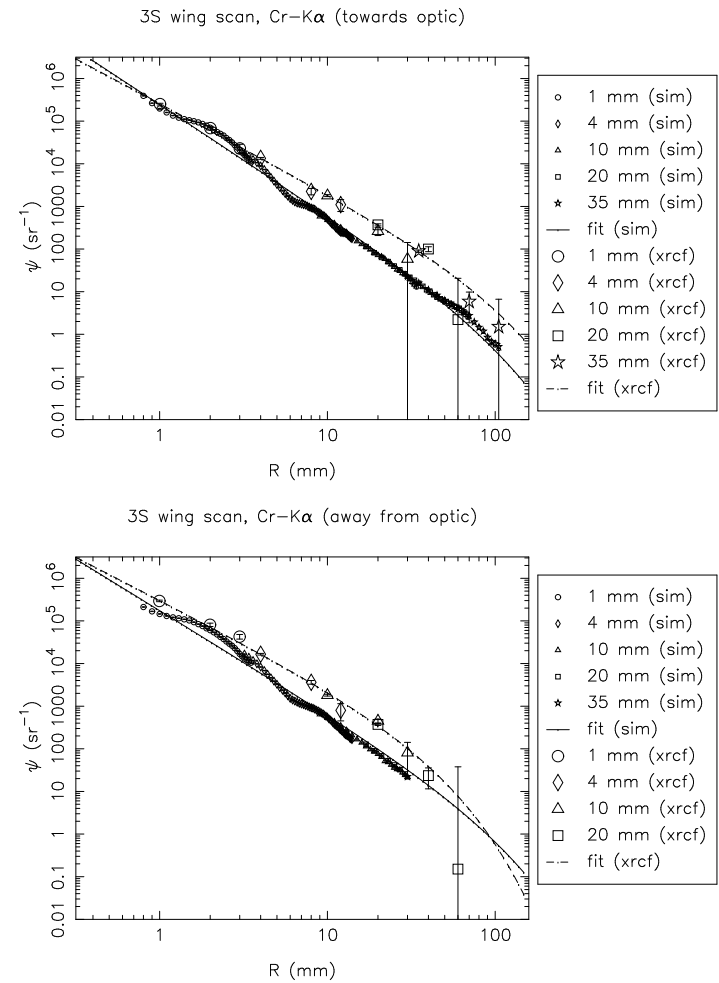


Figure 15.14: Shell 3S: Cr-K $\alpha$  surface brightness, towards and away from the optic

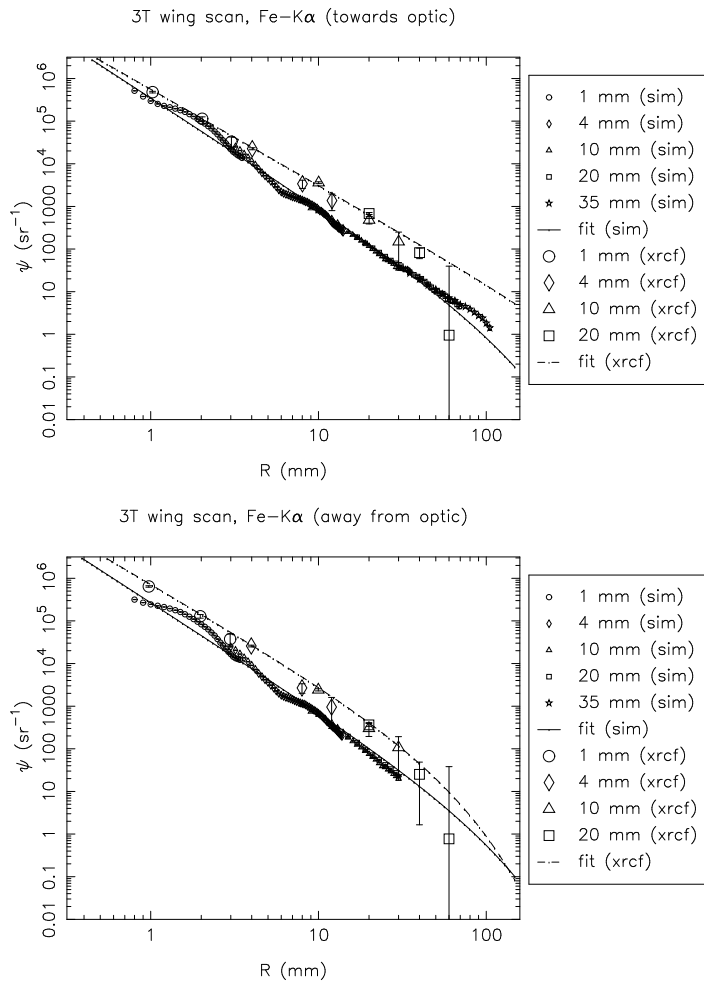


Figure 15.15: Shell 3T: Fe-K $\alpha$  surface brightness, towards and away from the optic

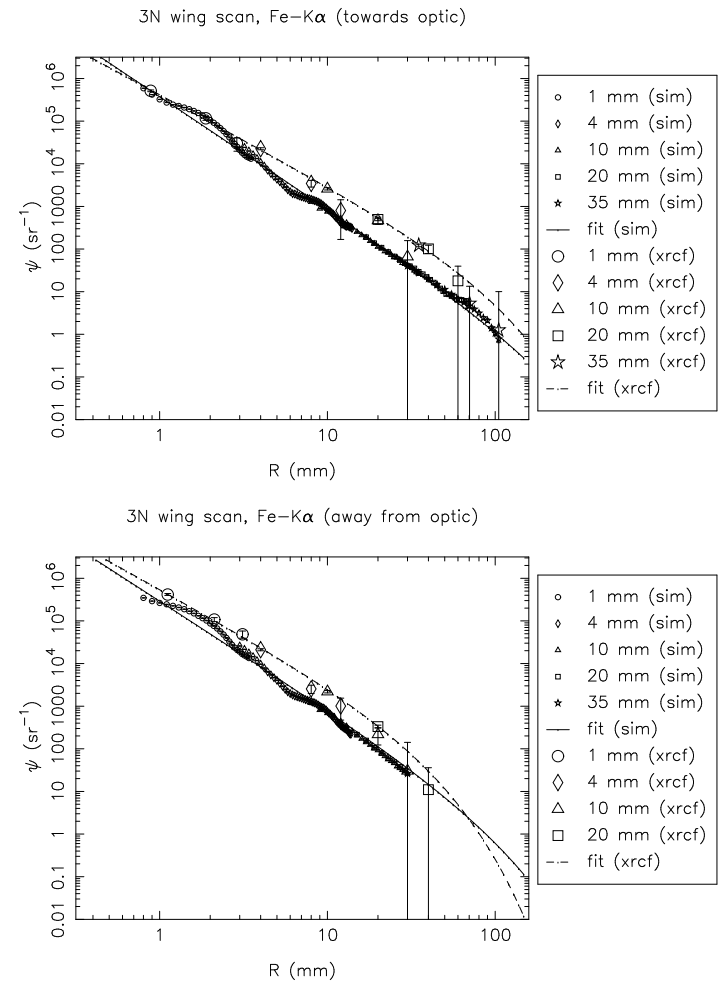


Figure 15.16: Shell 3N: Fe-K $\alpha$  surface brightness, towards and away from the optic

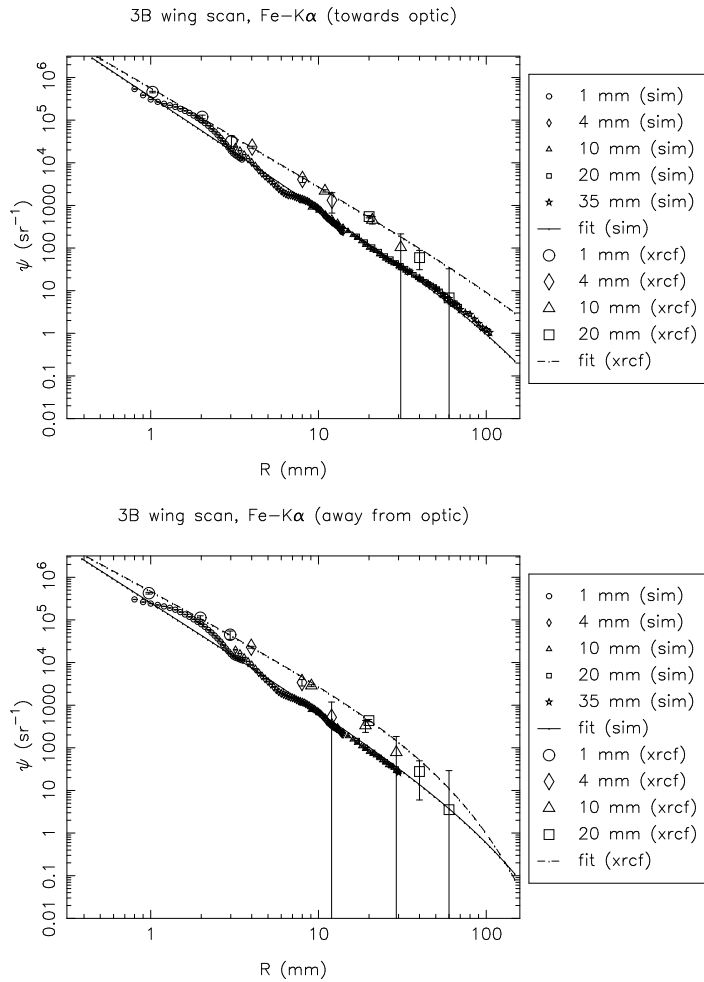


Figure 15.17: Shell 3B: Fe-K $\alpha$  surface brightness, towards and away from the optic

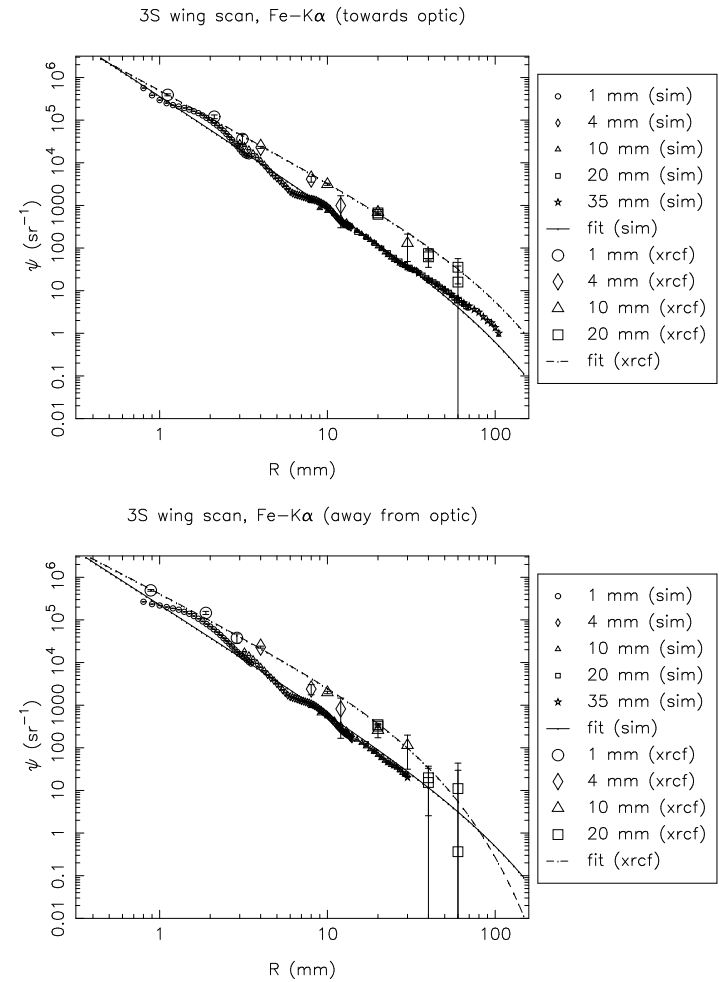


Figure 15.18: Shell 3S: Fe-K $\alpha$  surface brightness, towards and away from the optic

## 15.2.3 Shell 4 scans

Table 15.5: Surface brightness fits and fractional excess effective area beyond the 35 mm pinhole. (Raytrace simulations, Shell 4)

| Type | Quad | Line | Dir | a          | b     | c         | fractional extra area |
|------|------|------|-----|------------|-------|-----------|-----------------------|
| sim  | 4T   | Al   | in  | 45522.100  | 2.862 | 10000.000 | 0.000143              |
| sim  | 4T   | Al   | out | 29538.700  | 2.500 | 10000.000 | 0.000535              |
| sim  | 4N   | Al   | in  | 133732.000 | 3.433 | 10000.000 | 0.000034              |
| sim  | 4N   | Al   | out | 72861.700  | 2.880 | 10000.000 | 0.000209              |
| sim  | 4B   | Al   | in  | 155290.000 | 3.686 | 10000.000 | 0.000014              |
| sim  | 4B   | Al   | out | 54287.800  | 2.719 | 10000.000 | 0.000333              |
| sim  | 4S   | Al   | in  | 48438.200  | 2.912 | 10000.000 | 0.000120              |
| sim  | 4S   | Al   | out | 23695.800  | 2.435 | 10000.000 | 0.000601              |
| sim  | 4S   | Ti   | in  | 207308.000 | 2.531 | 278.904   | 0.001804              |
| sim  | 4S   | Ti   | out | 148785.000 | 2.320 | 85.397    | 0.001574              |
| sim  | 4S   | Cr   | in  | 271072.000 | 2.517 | 597.682   | 0.003174              |
| sim  | 4S   | Cr   | out | 200191.000 | 2.321 | 70.615    | 0.001770              |
| sim  | 4T   | Fe   | in  | 309523.000 | 2.447 | 600.865   | 0.005007              |
| sim  | 4T   | Fe   | out | 254766.000 | 2.354 | 70.000    | 0.001953              |
| sim  | 4N   | Fe   | in  | 420038.000 | 2.549 | 8658.530  | 0.005870              |
| sim  | 4N   | Fe   | out | 330389.000 | 2.390 | 70.000    | 0.002183              |
| sim  | 4B   | Fe   | in  | 457006.000 | 2.622 | 10000.000 | 0.004478              |
| sim  | 4B   | Fe   | out | 284517.000 | 2.365 | 70.000    | 0.002078              |
| sim  | 4S   | Fe   | in  | 330882.000 | 2.487 | 5767.630  | 0.006168              |
| sim  | 4S   | Fe   | out | 222297.000 | 2.317 | 70.000    | 0.001980              |
| sim  | 4S   | Cu   | in  | 489937.000 | 2.355 | 10000.000 | 0.018923              |
| sim  | 4S   | Cu   | out | 316625.000 | 2.401 | 95.931    | 0.002631              |

Table 15.6: Surface brightness fits and fractional excess effective area beyond the 35 mm pinhole. (XRCF data, Shell 4)

| Type | Quad | Line | Dir | a           | b     | c         | fractional extra area |
|------|------|------|-----|-------------|-------|-----------|-----------------------|
| xrcf | 4T   | Al   | in  | 113177.000  | 2.656 | 10000.000 | 0.000940              |
| xrcf | 4T   | Al   | out | 90027.300   | 2.756 | 10000.000 | 0.000462              |
| xrcf | 4N   | Al   | in  | 64983.900   | 2.475 | 6510.170  | 0.001299              |
| xrcf | 4N   | Al   | out | 67406.900   | 2.523 | 10000.000 | 0.001084              |
| xrcf | 4B   | Al   | in  | 163766.000  | 2.881 | 10000.000 | 0.000469              |
| xrcf | 4B   | Al   | out | 88631.200   | 2.352 | 89.746    | 0.000857              |
| xrcf | 4S   | Al   | in  | 37857.300   | 2.152 | 77.512    | 0.000741              |
| xrcf | 4S   | Al   | out | 106539.000  | 2.529 | 10000.000 | 0.001662              |
| xrcf | 4S   | Ti   | in  | 281656.000  | 2.156 | 54.267    | 0.003672              |
| xrcf | 4S   | Ti   | out | 222767.000  | 2.077 | 91.891    | 0.007020              |
| xrcf | 4S   | Cr   | in  | 311700.000  | 2.121 | 57.218    | 0.005000              |
| xrcf | 4S   | Cr   | out | 323288.000  | 2.089 | 47.867    | 0.004719              |
| xrcf | 4T   | Fe   | in  | 575581.000  | 2.220 | 85.123    | 0.009246              |
| xrcf | 4T   | Fe   | out | 576353.000  | 2.161 | 33.536    | 0.003687              |
| xrcf | 4N   | Fe   | in  | 462355.000  | 2.123 | 51.746    | 0.006503              |
| xrcf | 4N   | Fe   | out | 504010.000  | 2.151 | 47.334    | 0.005633              |
| xrcf | 4B   | Fe   | in  | 593296.000  | 2.317 | 184.370   | 0.010897              |
| xrcf | 4B   | Fe   | out | 549030.000  | 2.131 | 31.303    | 0.003510              |
| xrcf | 4S   | Fe   | in  | 476664.000  | 2.171 | 46.147    | 0.004748              |
| xrcf | 4S   | Fe   | out | 406663.000  | 1.985 | 19.077    | 0.001580              |
| xrcf | 4S   | Cu   | in  | 842582.000  | 1.885 | 42.887    | 0.024146              |
| xrcf | 4S   | Cu   | out | 1173790.000 | 2.335 | 48.786    | 0.006481              |

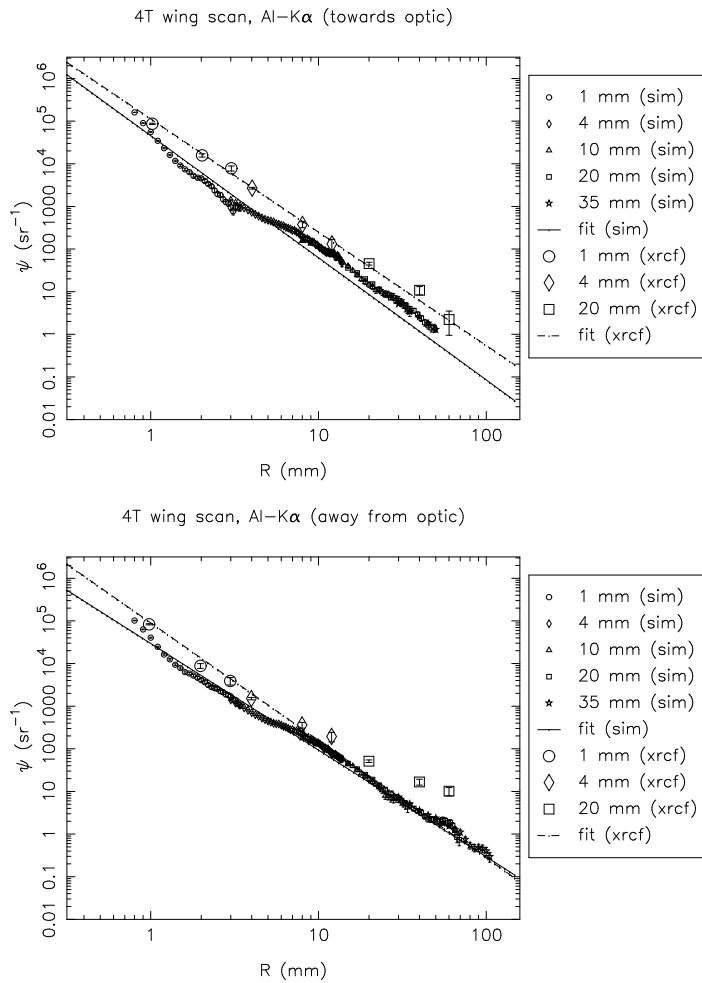


Figure 15.19: Shell 4T: Al-K $\alpha$  surface brightness, towards and away from the optic

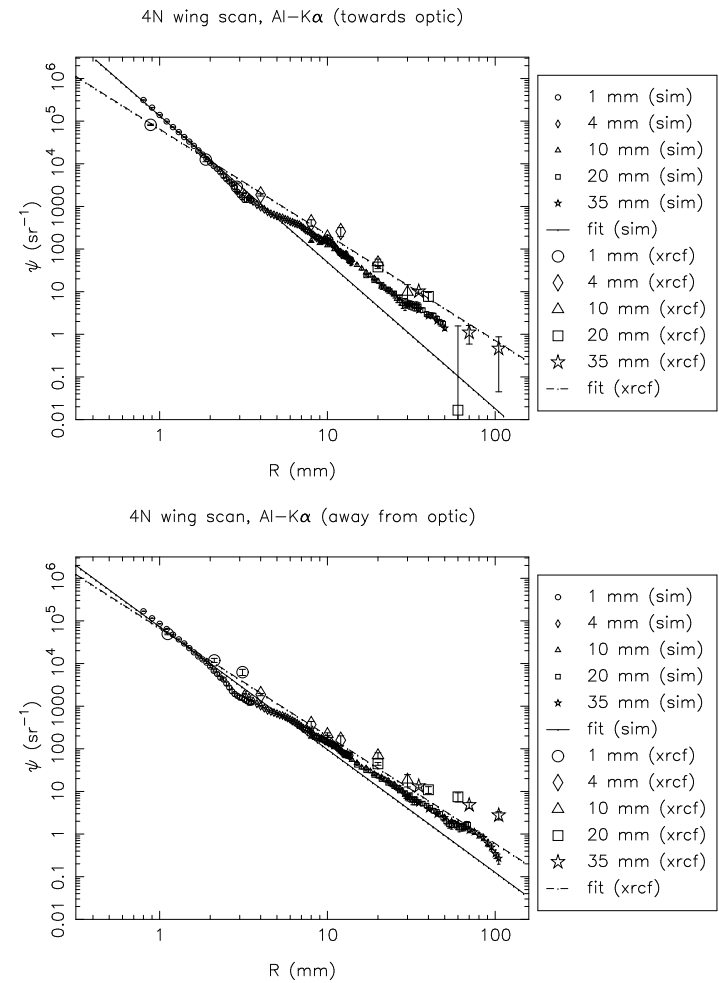


Figure 15.20: Shell 4N: Al-K $\alpha$  surface brightness, towards and away from the optic

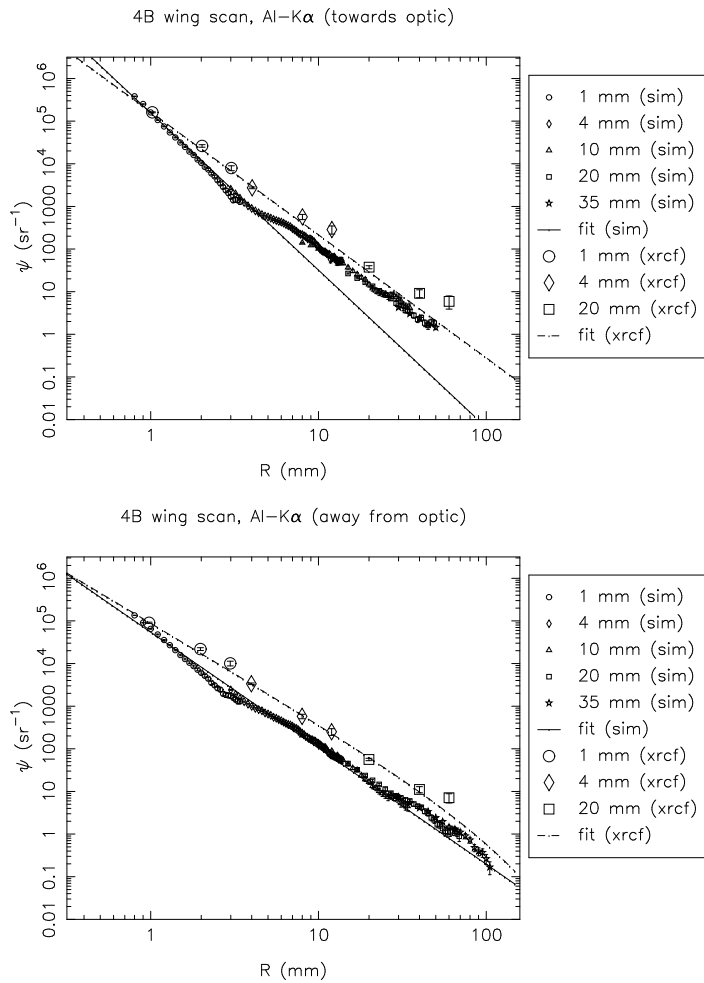


Figure 15.21: Shell 4B: Al-K $\alpha$  surface brightness, towards and away from the optic

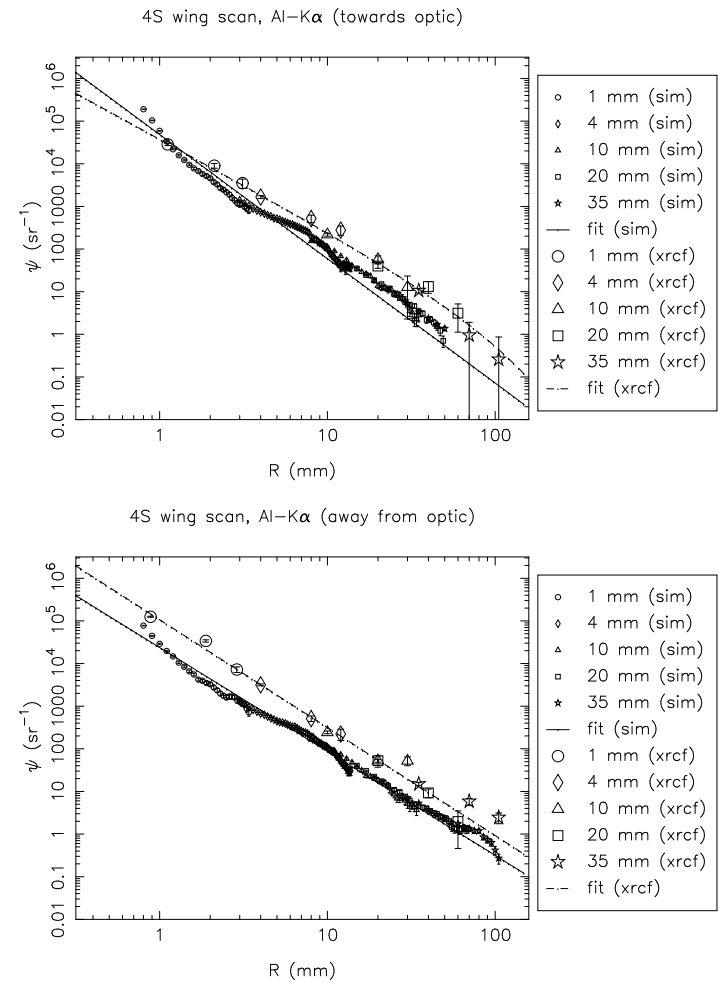


Figure 15.22: Shell 4S: Al-K $\alpha$  surface brightness, towards and away from the optic

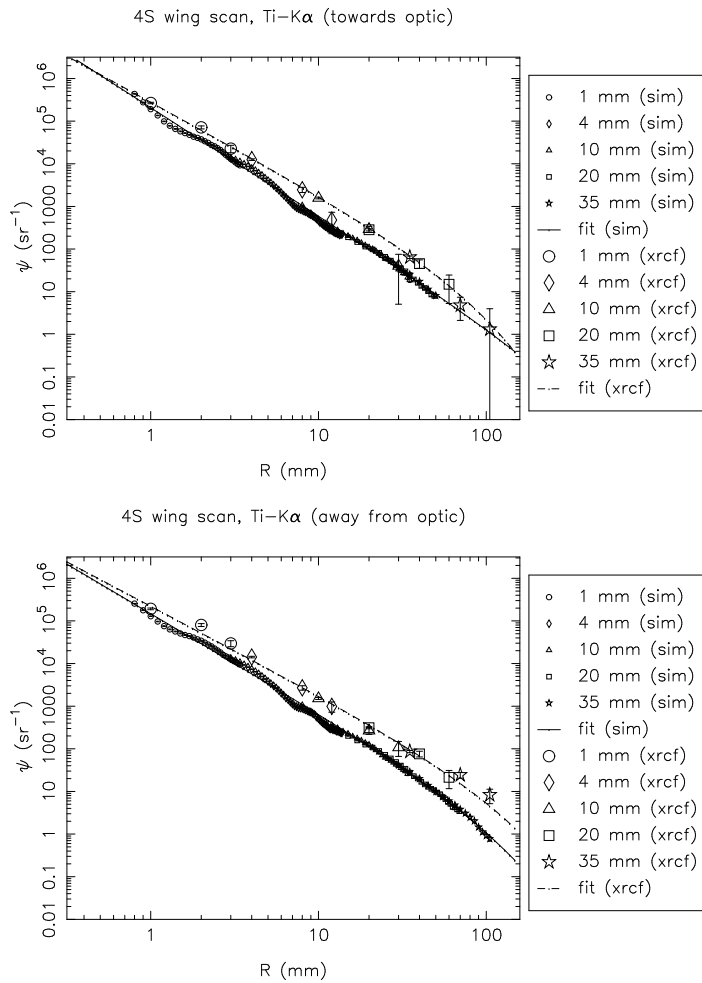


Figure 15.23: Shell 4S: Ti-K $\alpha$  surface brightness, towards and away from the optic

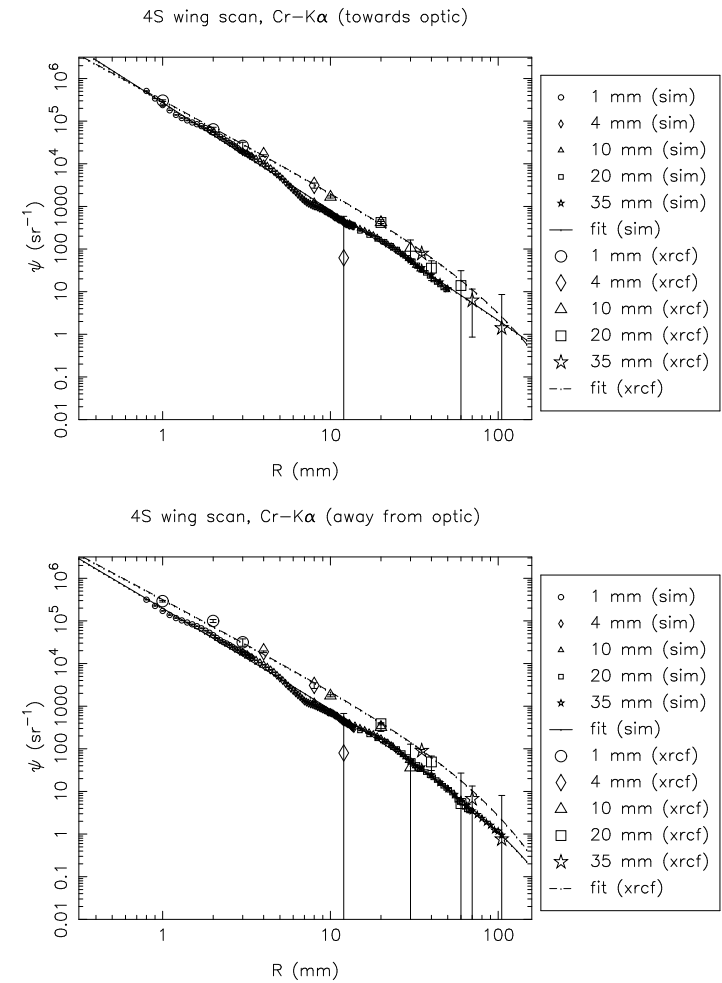


Figure 15.24: Shell 4S: Cr-K $\alpha$  surface brightness, towards and away from the optic

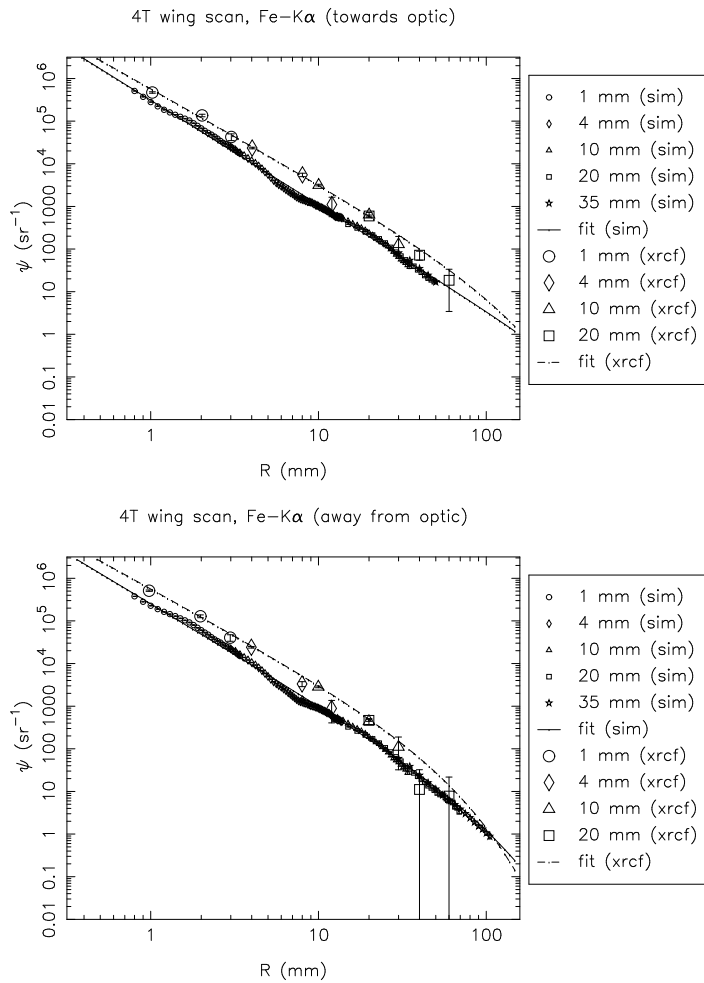


Figure 15.25: Shell 4T: Fe-K $\alpha$  surface brightness, towards and away from the optic

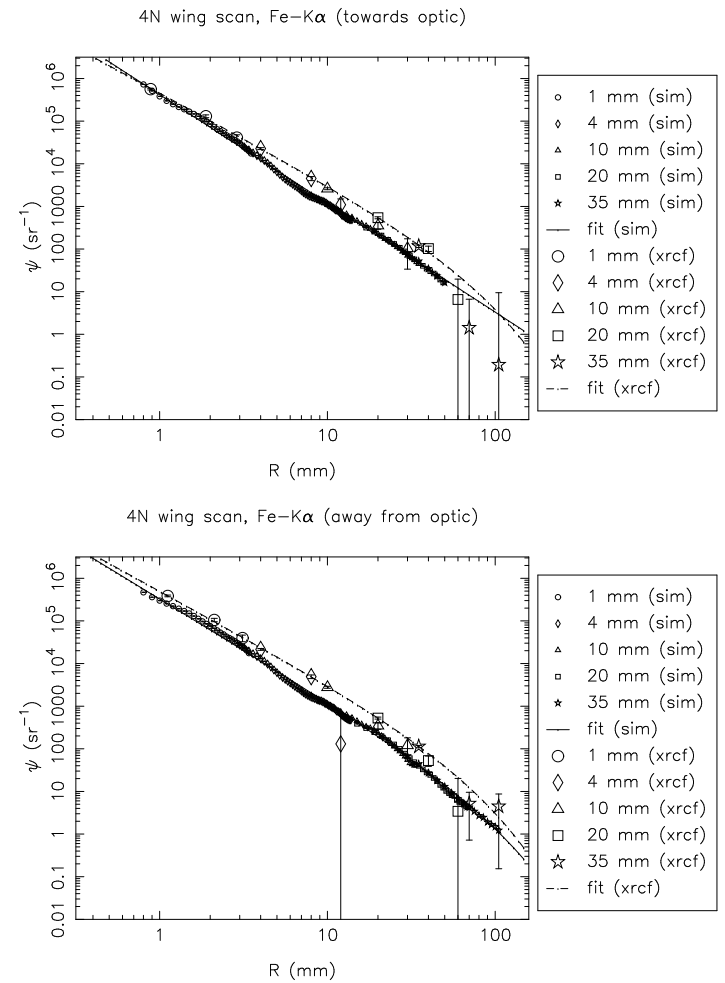


Figure 15.26: Shell 4N: Fe-K $\alpha$  surface brightness, towards and away from the optic

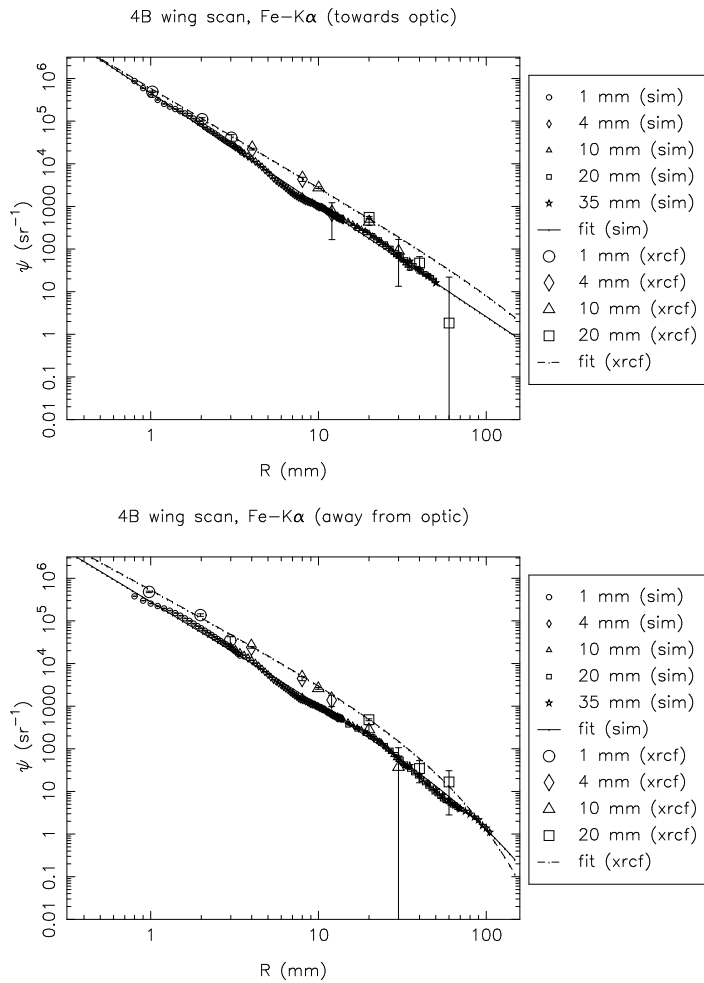


Figure 15.27: Shell 4B: Fe-K $\alpha$  surface brightness, towards and away from the optic

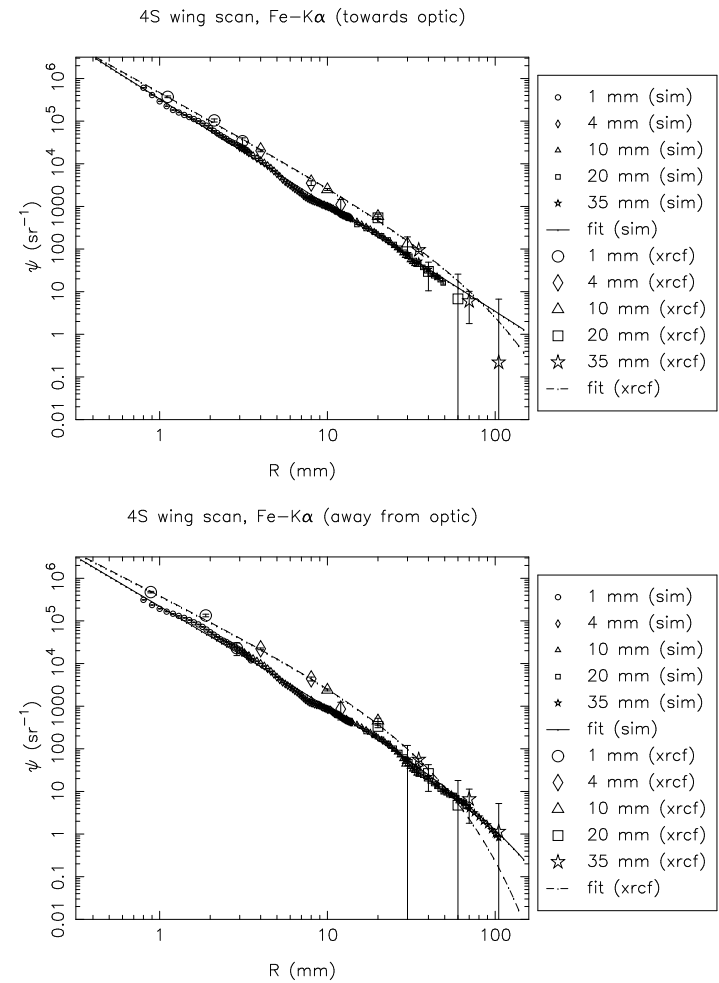


Figure 15.28: Shell 4S: Fe-K $\alpha$  surface brightness, towards and away from the optic

15.2.4 Shell 6 scans

Table 15.7: Surface brightness fits and fractional excess effective area beyond the 35 mm pinhole. (Raytrace simulations, Shell 6)

| Type | Quad | Line | Dir | a          | b     | c         | fractional extra area |
|------|------|------|-----|------------|-------|-----------|-----------------------|
| sim  | 6B   | C    | in  | 25912.900  | 3.142 | 70.000    | 0.000008              |
| sim  | 6B   | C    | out | 30915.300  | 2.895 | 70.000    | 0.000026              |
| sim  | 6T   | Al   | in  | 121092.000 | 3.146 | 10000.000 | 0.000105              |
| sim  | 6T   | Al   | out | 116395.000 | 3.095 | 10000.000 | 0.000127              |
| sim  | 6N   | Al   | in  | 101486.600 | 3.262 | 10000.000 | 0.000053              |
| sim  | 6N   | Al   | out | 120531.000 | 3.058 | 10000.000 | 0.000155              |
| sim  | 6B   | Al   | in  | 122030.000 | 3.475 | 10000.000 | 0.000026              |
| sim  | 6B   | Al   | out | 109760.000 | 3.109 | 10000.000 | 0.000112              |
| sim  | 6S   | Al   | in  | 134708.000 | 3.231 | 10000.000 | 0.000081              |
| sim  | 6S   | Al   | out | 96170.800  | 3.019 | 10000.000 | 0.000147              |
| sim  | 6S   | Ti   | in  | 199568.000 | 2.518 | 70.000    | 0.000779              |
| sim  | 6S   | Ti   | out | 193288.000 | 2.421 | 70.000    | 0.001121              |
| sim  | 6S   | Cr   | in  | 246680.000 | 2.482 | 70.000    | 0.001115              |
| sim  | 6S   | Cr   | out | 232063.000 | 2.388 | 70.000    | 0.001543              |
| sim  | 6T   | Fe   | in  | 292414.000 | 2.415 | 70.000    | 0.001741              |
| sim  | 6T   | Fe   | out | 284040.000 | 2.373 | 70.000    | 0.002010              |
| sim  | 6N   | Fe   | in  | 298852.000 | 2.414 | 70.000    | 0.001789              |
| sim  | 6N   | Fe   | out | 305030.000 | 2.354 | 70.000    | 0.002333              |
| sim  | 6B   | Fe   | in  | 335773.000 | 2.506 | 70.000    | 0.001378              |
| sim  | 6B   | Fe   | out | 279676.000 | 2.356 | 70.000    | 0.002125              |
| sim  | 6S   | Fe   | in  | 317636.000 | 2.464 | 70.000    | 0.001548              |
| sim  | 6S   | Fe   | out | 246516.000 | 2.352 | 70.000    | 0.001903              |
| sim  | 6T   | Cu   | in  | 388002.000 | 2.394 | 70.000    | 0.002519              |
| sim  | 6T   | Cu   | out | 383320.000 | 2.453 | 70.000    | 0.001953              |
| sim  | 6N   | Cu   | in  | 415306.000 | 2.415 | 70.000    | 0.002471              |
| sim  | 6N   | Cu   | out | 417002.000 | 2.436 | 70.000    | 0.002275              |
| sim  | 6B   | Cu   | in  | 442238.000 | 2.470 | 70.000    | 0.002105              |
| sim  | 6B   | Cu   | out | 387613.000 | 2.437 | 70.000    | 0.002108              |
| sim  | 6S   | Cu   | in  | 431805.000 | 2.439 | 70.000    | 0.002333              |
| sim  | 6S   | Cu   | out | 330644.000 | 2.368 | 70.000    | 0.002390              |

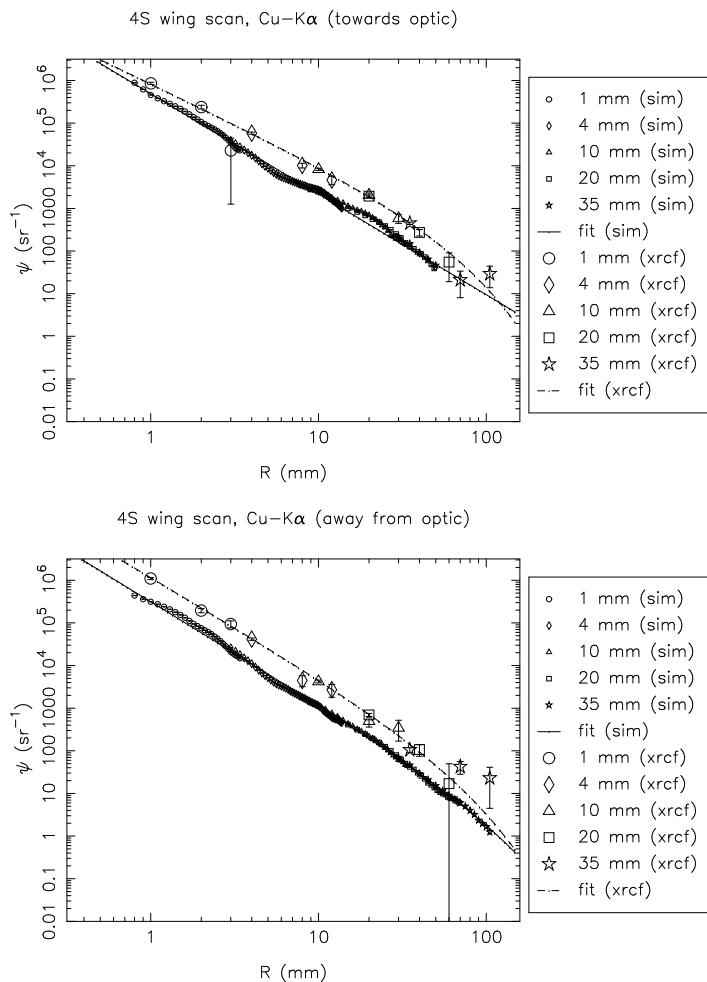


Figure 15.29: Shell 4S: Cu-K $\alpha$  surface brightness, towards and away from the optic

Table 15.8: Surface brightness fits and fractional excess effective area beyond the 35 mm pinhole. (XRCF data, Shell 6)

| Type | Quad | Line | Dir | a          | b     | c         | fractional extra area |
|------|------|------|-----|------------|-------|-----------|-----------------------|
| xrcf | 6B   | C    | in  | 107596.000 | 2.926 | 50.000    | 0.000058              |
| xrcf | 6B   | C    | out | 61652.600  | 2.939 | 50.000    | 0.000031              |
| xrcf | 6T   | Al   | in  | 76735.100  | 2.176 | 12.628    | 0.000041              |
| xrcf | 6T   | Al   | out | 194262.000 | 3.076 | 10000.000 | 0.000230              |
| xrcf | 6N   | Al   | in  | 103493.200 | 2.751 | 10000.000 | 0.000544              |
| xrcf | 6N   | Al   | out | 169376.000 | 2.860 | 10000.000 | 0.000534              |
| xrcf | 6B   | Al   | in  | 168171.000 | 2.846 | 10000.000 | 0.000566              |
| xrcf | 6B   | Al   | out | 103630.200 | 2.655 | 10000.000 | 0.000865              |
| xrcf | 6S   | Al   | in  | 193325.000 | 3.605 | 10000.000 | 0.000024              |
| xrcf | 6S   | Al   | out | 209454.000 | 2.982 | 10000.000 | 0.000378              |
| xrcf | 6S   | Ti   | in  | 255254.000 | 2.216 | 98.125    | 0.004716              |
| xrcf | 6S   | Ti   | out | 222456.000 | 2.161 | 76.943    | 0.004162              |
| xrcf | 6S   | Cr   | in  | 258517.000 | 2.108 | 46.722    | 0.003380              |
| xrcf | 6S   | Cr   | out | 284988.000 | 2.073 | 38.094    | 0.003186              |
| xrcf | 6T   | Fe   | in  | 286282.000 | 1.911 | 35.797    | 0.005547              |
| xrcf | 6T   | Fe   | in  | 418386.000 | 2.104 | 40.853    | 0.004595              |
| xrcf | 6T   | Fe   | out | 286282.000 | 1.911 | 35.797    | 0.005547              |
| xrcf | 6T   | Fe   | out | 418386.000 | 2.104 | 40.853    | 0.004595              |
| xrcf | 6N   | Fe   | in  | 284232.000 | 1.840 | 19.108    | 0.001944              |
| xrcf | 6N   | Fe   | out | 360357.000 | 2.108 | 46.673    | 0.004705              |
| xrcf | 6B   | Fe   | in  | 421488.000 | 2.182 | 55.439    | 0.005070              |
| xrcf | 6B   | Fe   | out | 376848.000 | 2.039 | 36.442    | 0.004500              |
| xrcf | 6S   | Fe   | in  | 399255.000 | 2.052 | 38.782    | 0.004994              |
| xrcf | 6S   | Fe   | out | 309988.000 | 1.994 | 36.596    | 0.004464              |
| xrcf | 6T   | Cu   | in  | 426542.000 | 1.872 | 24.960    | 0.004861              |
| xrcf | 6T   | Cu   | out | 511460.000 | 1.981 | 20.652    | 0.002465              |
| xrcf | 6N   | Cu   | in  | 478480.000 | 1.807 | 14.549    | 0.001680              |
| xrcf | 6N   | Cu   | out | 478914.000 | 1.917 | 17.547    | 0.001933              |
| xrcf | 6B   | Cu   | in  | 548984.000 | 2.065 | 32.972    | 0.004997              |
| xrcf | 6B   | Cu   | out | 478089.000 | 1.893 | 19.165    | 0.002684              |
| xrcf | 6S   | Cu   | in  | 467525.000 | 1.887 | 19.009    | 0.002630              |
| xrcf | 6S   | Cu   | out | 483961.000 | 1.957 | 15.265    | 0.001114              |

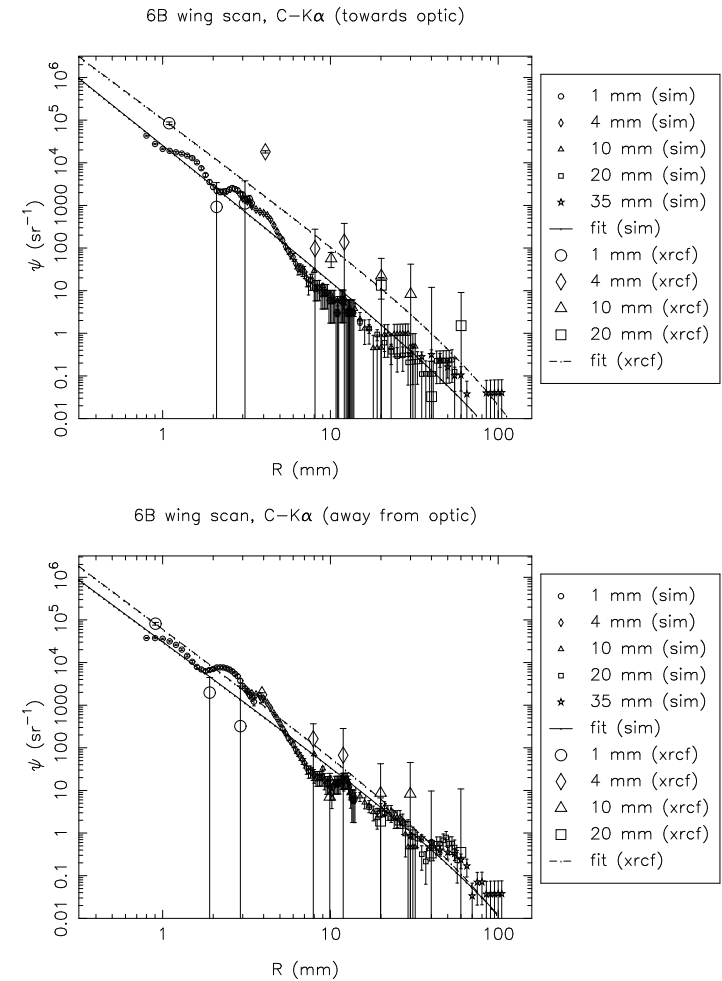


Figure 15.30: Shell 6B: C-K $\alpha$  surface brightness, towards and away from the optic

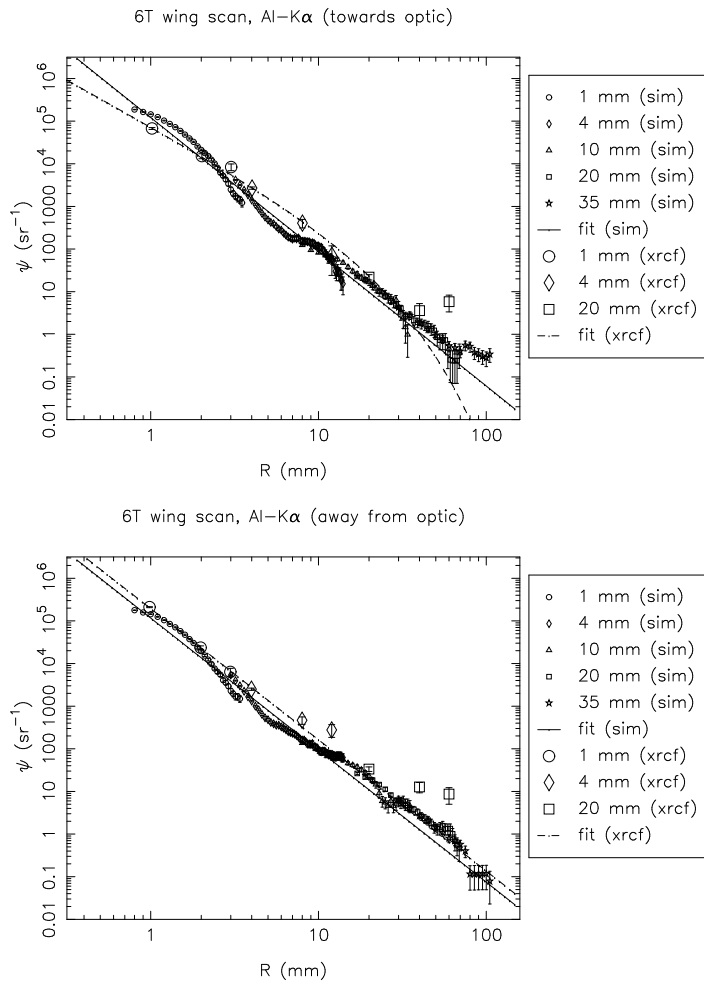


Figure 15.31: Shell 6T: Al-K $\alpha$  surface brightness, towards and away from the optic

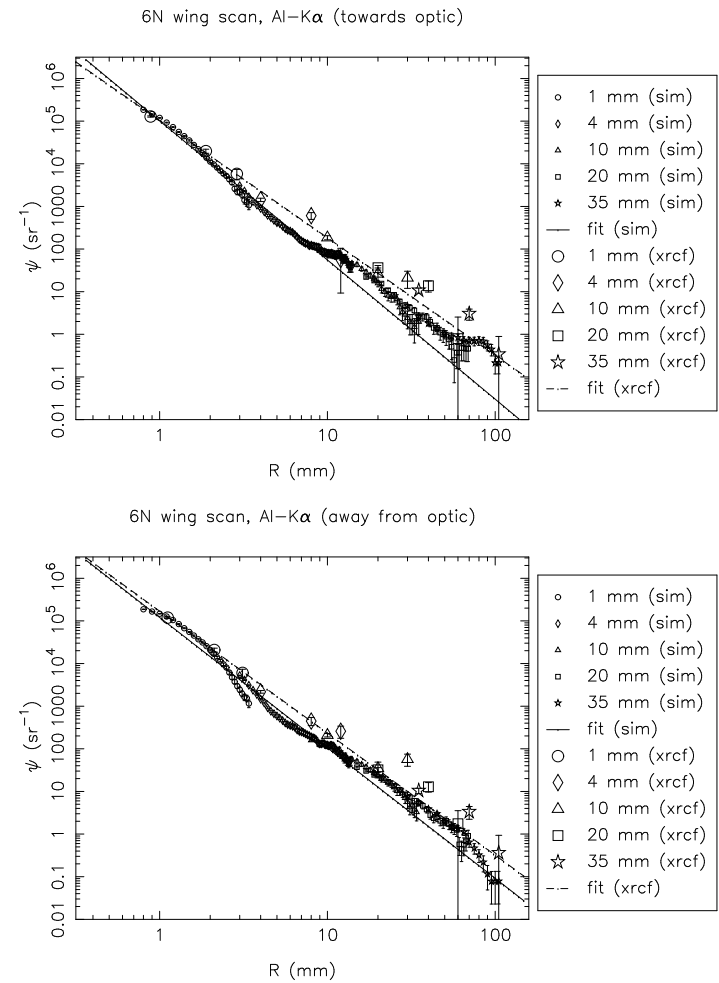


Figure 15.32: Shell 6N: Al-K $\alpha$  surface brightness, towards and away from the optic

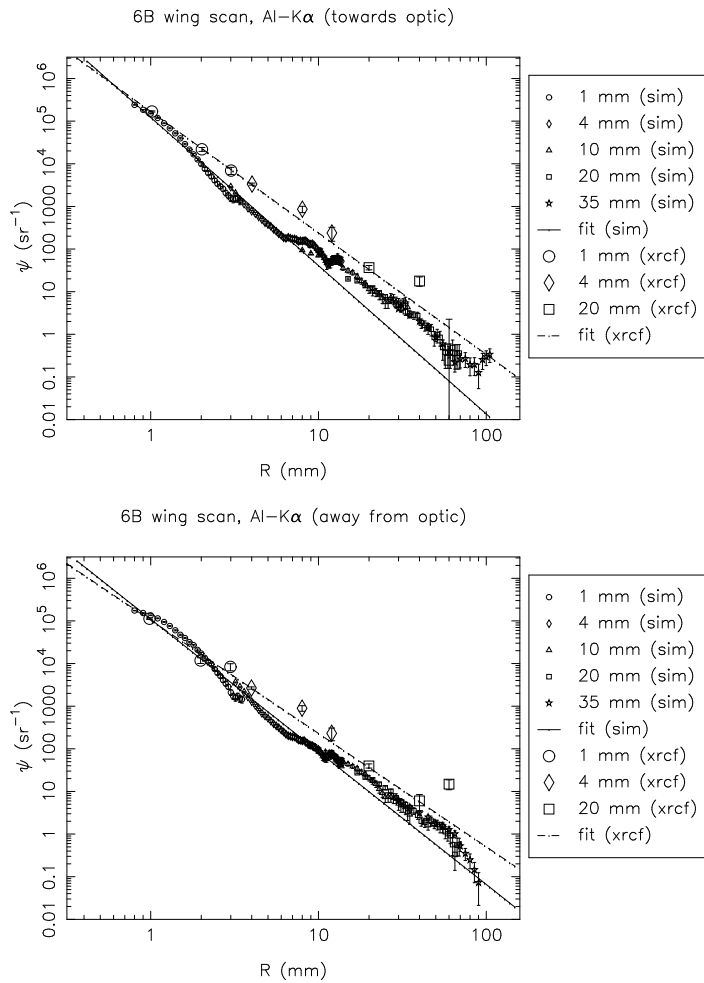


Figure 15.33: Shell 6B: Al-K $\alpha$  surface brightness, towards and away from the optic

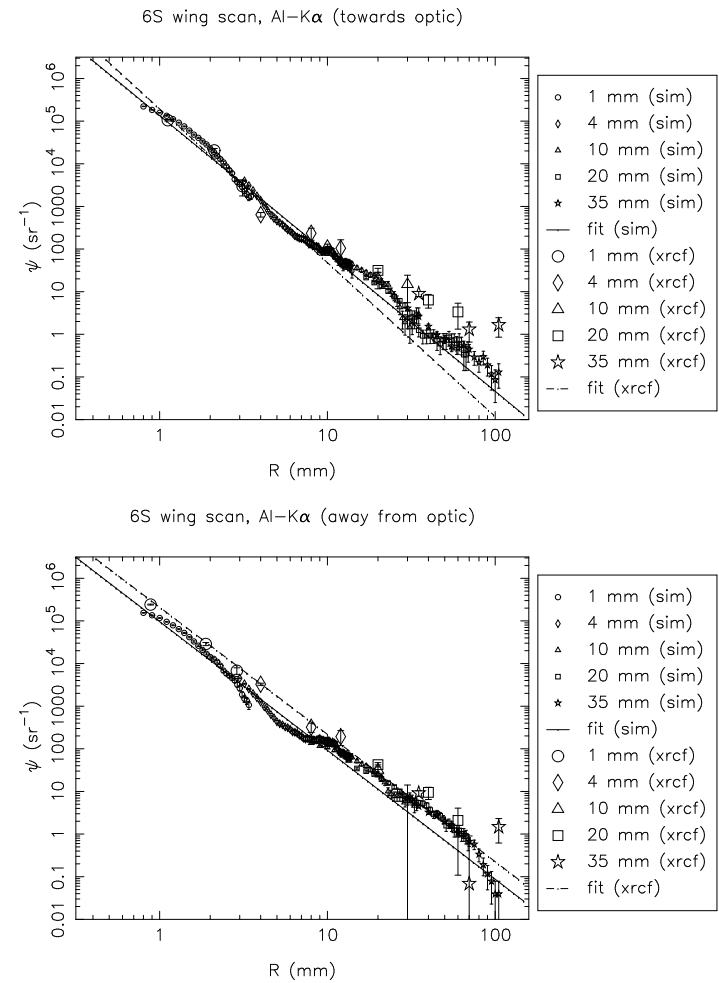


Figure 15.34: Shell 6S: Al-K $\alpha$  surface brightness, towards and away from the optic

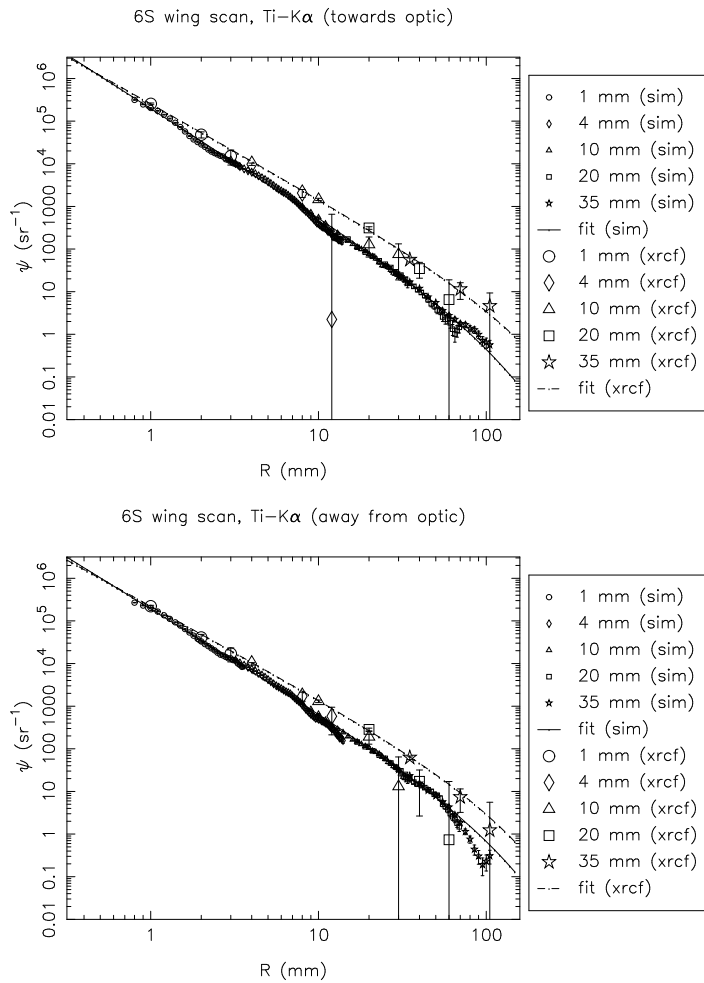


Figure 15.35: Shell 6S: Ti-K $\alpha$  surface brightness, towards and away from the optic

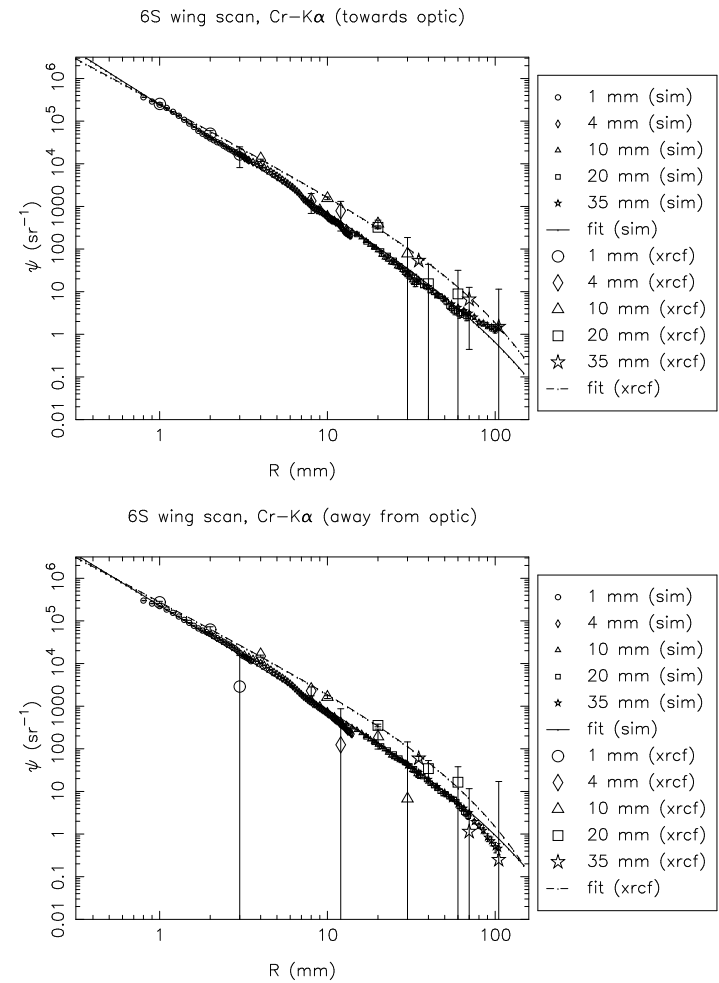


Figure 15.36: Shell 6S: Cr-K $\alpha$  surface brightness, towards and away from the optic

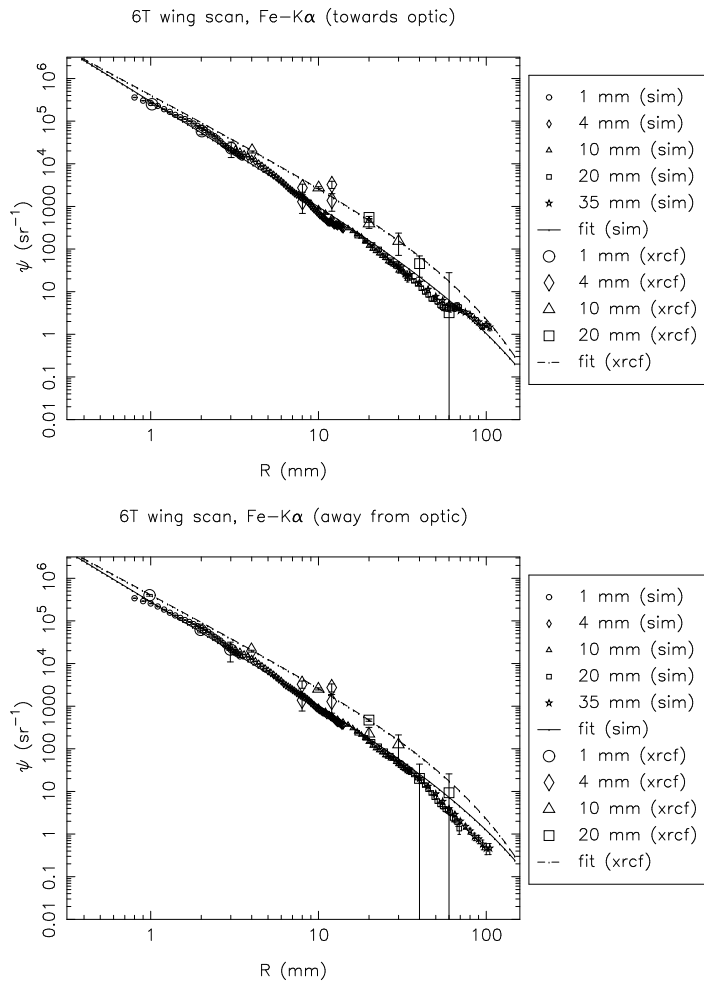


Figure 15.37: Shell 6T: Fe-K $\alpha$  surface brightness, towards and away from the optic

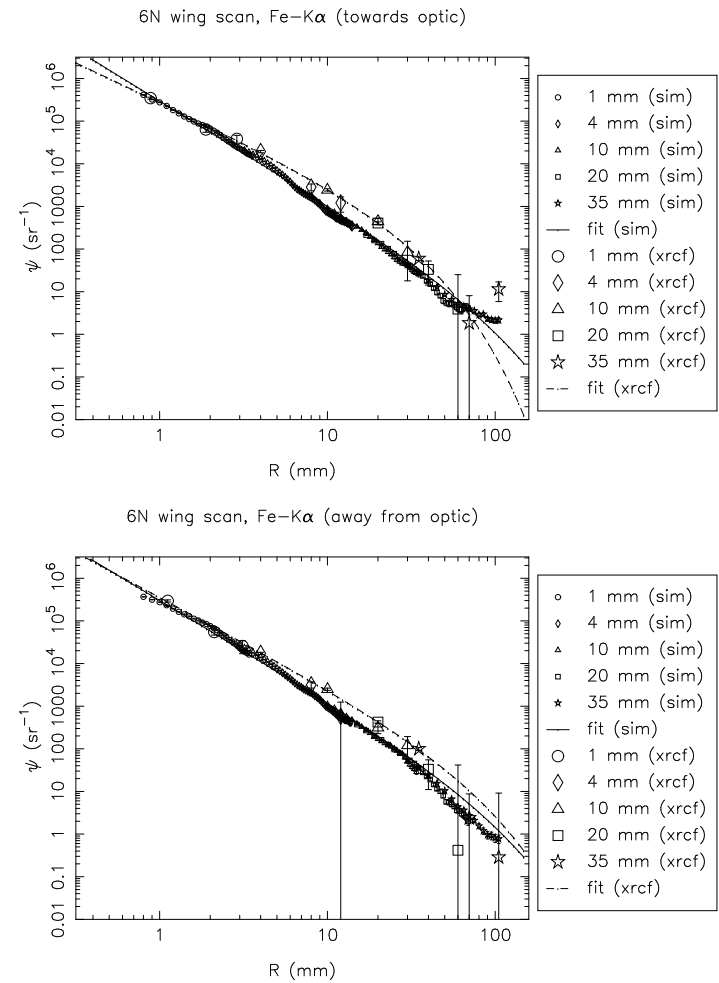


Figure 15.38: Shell 6N: Fe-K $\alpha$  surface brightness, towards and away from the optic

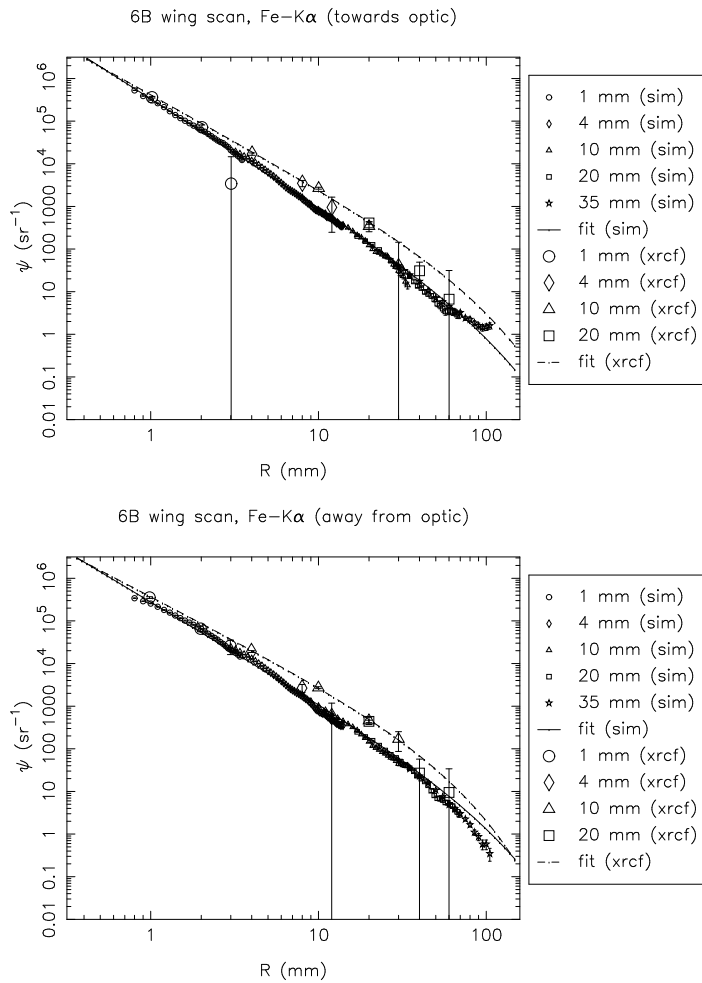


Figure 15.39: Shell 6B: Fe-K $\alpha$  surface brightness, towards and away from the optic

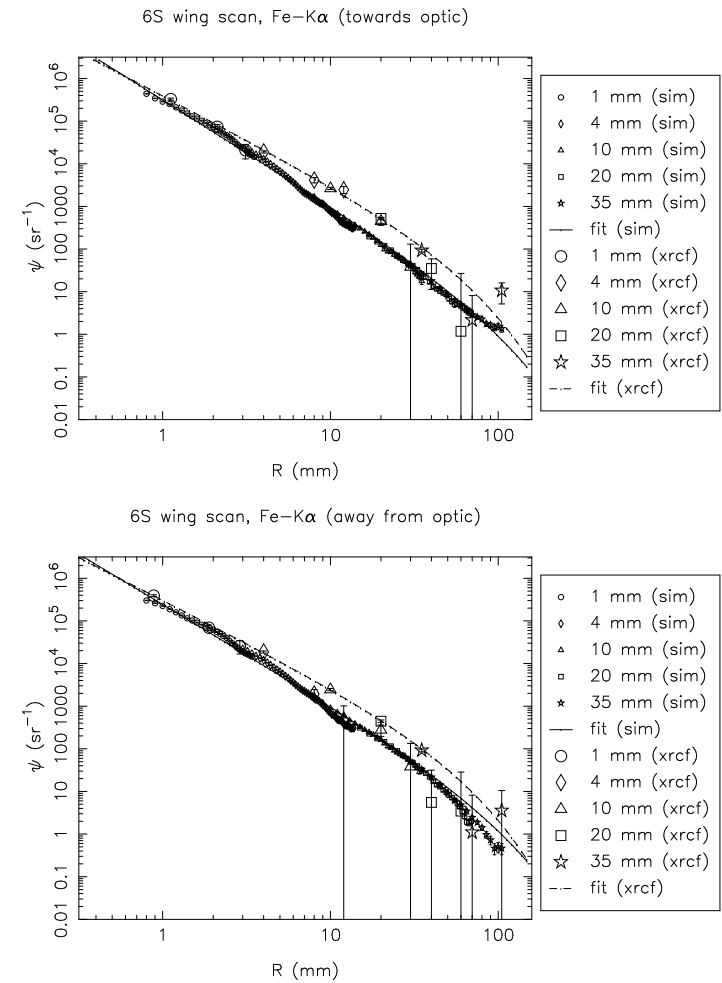


Figure 15.40: Shell 6S: Fe-K $\alpha$  surface brightness, towards and away from the optic

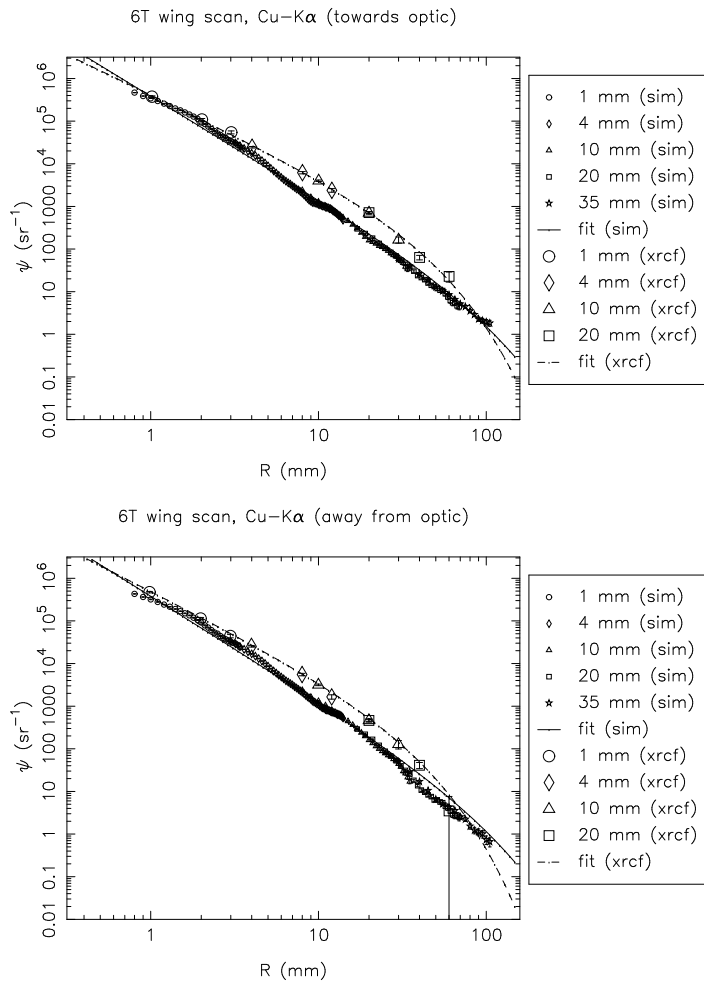


Figure 15.41: Shell 6T: Cu-K $\alpha$  surface brightness, towards and away from the optic

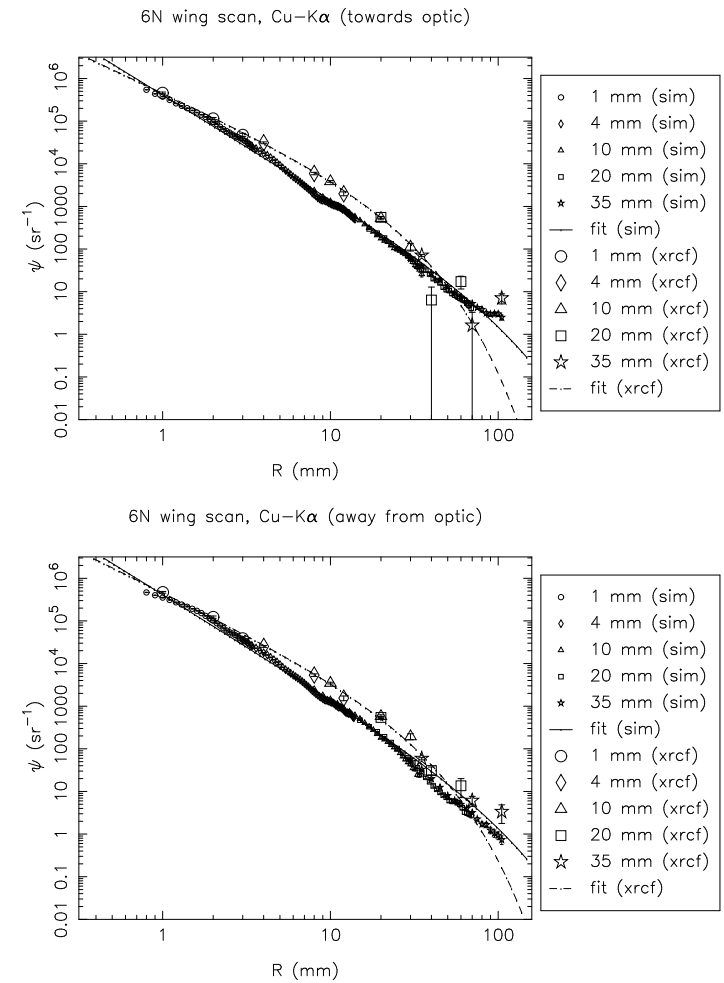


Figure 15.42: Shell 6N: Cu-K $\alpha$  surface brightness, towards and away from the optic

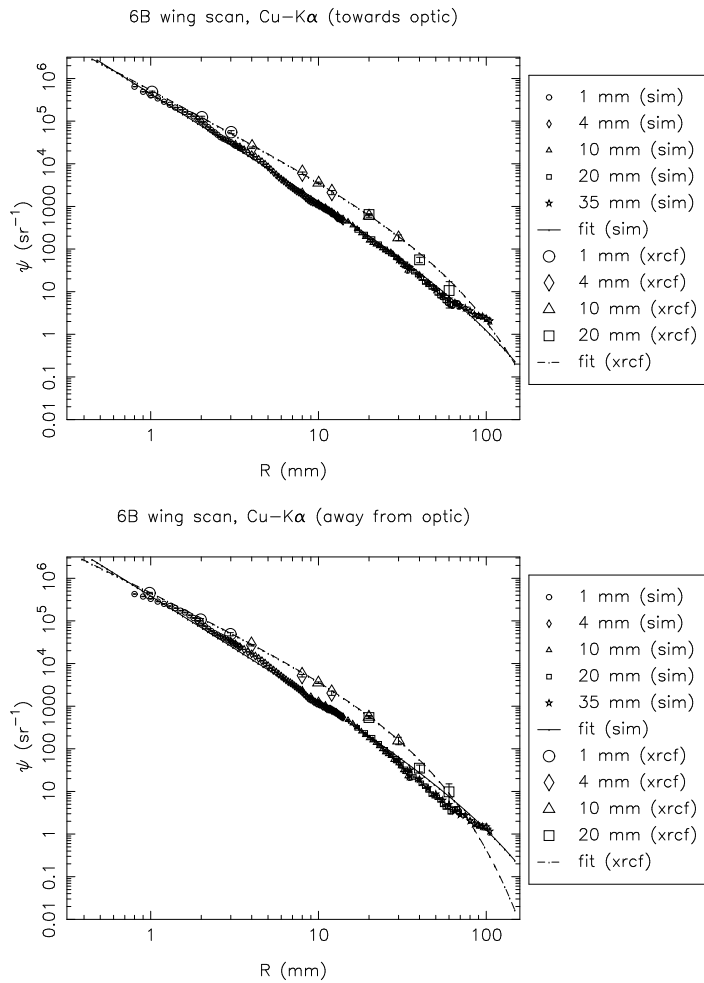


Figure 15.43: Shell 6B: Cu-K $\alpha$  surface brightness, towards and away from the optic

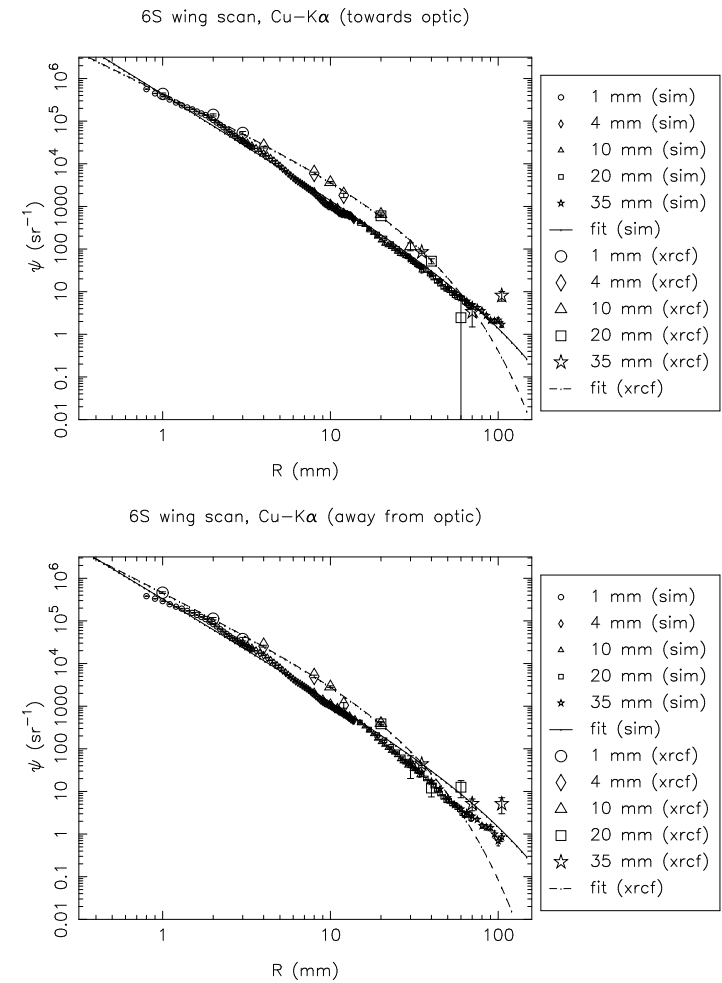


Figure 15.44: Shell 6S: Cu-K $\alpha$  surface brightness, towards and away from the optic

### 15.2.5 Double Quadrant Scans

Table 15.9: Surface brightness fits and fractional excess effective area beyond the 35 mm pinhole. (Raytrace simulations and XRCF data, Shell 4N 4S)

| Type | Quad | Line | Dir  | a          | b     | c         | fractional extra area |
|------|------|------|------|------------|-------|-----------|-----------------------|
| sim  | 4NS  | Al   | both | 202617.000 | 3.204 | 10000.000 | 0.000137              |
| xrcf | 4NS  | Al   | both | 254343.000 | 2.500 | 54.593    | 0.000825              |

Table 15.10: Surface brightness fits and fractional excess effective area beyond the 35 mm pinhole. (Raytrace simulations and XRCF data, Shell 6N 6S)

| Type | Quad | Line | Dir  | a          | b     | c         | fractional extra area |
|------|------|------|------|------------|-------|-----------|-----------------------|
| sim  | 6NS  | Al   | both | 195929.000 | 3.167 | 10000.000 | 0.000156              |
| xrcf | 6NS  | Al   | both | 236995.000 | 2.500 | 35.660    | 0.000437              |

The surface brightness profiles for the double-quadrant scans are presented in Figure 15.45.

## 15.3 Out-of-Plane Scattering

Two sets of wing scans were conducted for which the scan was transverse to the direction of the quadrant. The first was the set of 6B Y-scans performed at C-K $\alpha$ ; these scans were intended to look for signs of dust scattering. The scattering from microroughness is mainly in-plane, and an excess out-of-plane component might be produced by dust scattering. The second set of scans were the 3B Y-scans at Al-K $\alpha$ . These were performed in order to correct the double-quadrant wing scans (6N6S, 4N4S) for the fact that the 3B quadrant shutter was sticking and was open during the scans. The surface brightnesses based on these scans are plotted in Figure 15.46. For comparison, in-plane scans for the same shell and quadrant are also shown. Note, however, that the 3B out-of-plane scans were with HRMA at zero pitch and yaw, while the 3B in-plane scans were performed with HRMA yawed.

The out-of-plane component for the scattering due to microroughness is expected to be smaller than the in-plane component by a factor of order  $\sin \alpha$  where  $\alpha$  is the graze angle for the given shell. For shell 3 this factor would be about 1/83, while for shell 6 the factor would be about 1/130. The raytrace for the transverse scan for shell 6B at C-K $\alpha$  suggests that the raytrace model may be lower in wing surface brightness by perhaps a factor of 10; however, the raytrace has very few counts in the wings, and the 10 mm pinhole positions show no counts this far into the wings. Longer raytraces are needed before the questions can be answered definitively. It is also worth noting that in the current scattering model, the out-of-plane component is calculated as  $\sin \alpha$  times the in-plane component; this treatment may be too simplistic. The 3B out-of-plane scan data indicate a flatter slope than in the raytrace data, but this probably is not significant given the small number of data points and the large uncertainties in the values.

In Chapter 14, it was noted that the X-ray data for the 4 mm pinhole effective areas were peculiar in that the pinhole effective area for the position 4 mm to one side of the core was more than a factor of 10 larger than the corresponding position on the other side of the core (both for

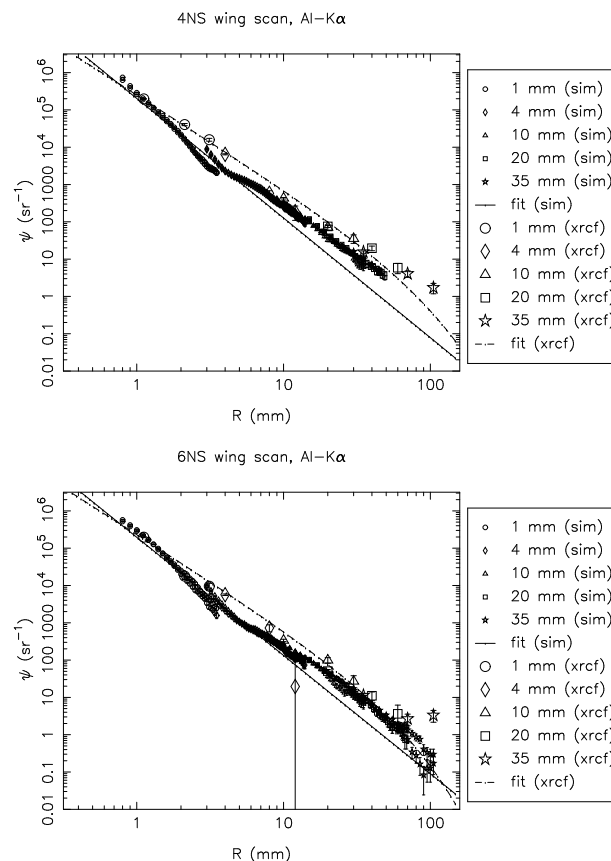


Figure 15.45: Double quadrant wing scan surface brightness: Al-K $\alpha$ . Top: Shell 4, N and S quadrant. Bottom: Shell 6, N and S quadrant.

the in-plane and out-of-plane cases). In Figure 15.46 these are the diamond-shaped points at  $R = 4$  mm.

## 15.4 Comparison with Encircled Energy Data

In order to show the consistency between the wing scan surface brightness data and the encircled energy data, we have plotted in Figure 15.47 the surface brightness profile measured in two different ways, for the one case for which this is feasible. The encircled energy tests are described in Chapter 16; these tests give a measurement of the surface brightness integrated out to the radius of a given aperture centered on the peak of the distribution, so numerically differentiating the effective area *vs.* radius curve gives us the surface brightness profile. In order to make a direct

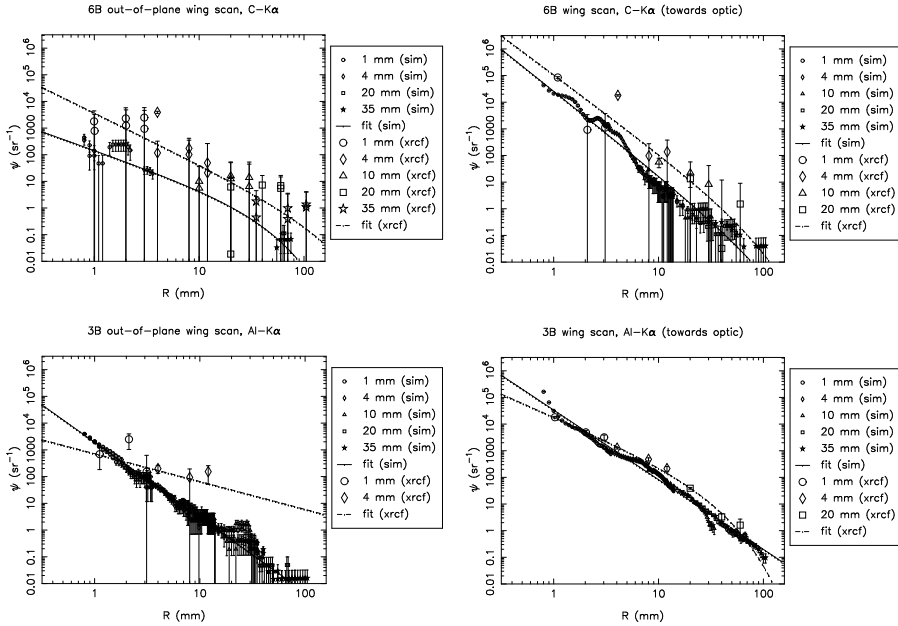


Figure 15.46: Out-of-plane scans, compared to in-plane scans. Top left: 6B Y scan at C-Kα (out of plane). Top right: 6B Z scan at C-Kα (in plane, towards optic). Bottom left: 3B Y scan at Al-Kα (out of plane). Bottom right: 3B Z scan at Al-Kα (in plane).

comparison with the wingscan surface brightness measurements, the surface brightness obtained by differentiating the effective area curve was scaled by a factor of  $2 \times 88/360$  times the effective area within an on-axis 35 mm diameter pinhole, to account for the fact that the wing scans were done one quadrant at a time (see §15.2). This surface brightness and that for the 1S Ti-Kα wing scan are plotted in Figure 15.47. The case of Ti K-α for Shell 1 is unique in that the encircled energy curve is both steep enough in the outer parts and well enough measured that the numerical derivative can be computed with finite error bars. Other cases examined showed the wing scan data at a level not inconsistent with the encircled energy data, but due to the large error bars on the latter, no stronger conclusions can be drawn. Note also the HRMA was yawed by  $-1'$  during this effective area experiment and by  $-4.56'$  in this wing scan measurement (see §D.7.2 and Table 14.3).

### 15.5 “2W<sub>1</sub>” Profiles

Finally, given the surface brightness profiles for various energies, the “2W<sub>1</sub>” functions describing the surface can be evaluated. The value of 2W<sub>1</sub> is based on equation (7) of O’Dell et al. (1992):

$$2W_1(f) \simeq \frac{f\psi(\theta)\lambda^4}{16\pi \sin^4 \alpha} \quad (15.9)$$

where  $f = \theta \sin \alpha / \lambda$  is the spatial frequency,  $\theta$  is the off-axis angle,  $\alpha$  is the mean graze angle for the mirror shell,  $\lambda$  is the X-ray wavelength, and  $\psi$  is the surface brightness normalized to a scaled on-axis effective area measured using the largest 35 mm pinhole (see §15.2 and also the MST preliminary report).

It should be emphasized that the PSD thus calculated is *per surface*.

The resulting 2W<sub>1</sub> data are fit with functions of the form

$$2W_1(f) = af^{-b}e^{-f/c}. \quad (15.10)$$

Again, the raytrace data are not fit well by this particular form; as for the surface brightness fits to the raytrace data, the exponential scale length parameter was limited to fall within a given range of values, in this case 190–10000. The lower limit (obtained by trial and error) was chosen to reproduce approximately the overall shape of the curve at large radii. As before, the overall shape fits reasonably well in some cases but not in others; in future analyses, different limit ranges should be applied on a case by case basis.

In the following tables and figures, the 2W<sub>1</sub> obtained from the X-ray data are compared to the 2W<sub>1</sub> based on the raytrace simulations.

The agreement between the XRCF data and the raytrace simulations seems to be generally better towards smaller  $f$  values. The agreement towards larger  $f$  gets significantly worse, particularly for the larger shells. The raytrace models for shell 6 indicate a high shoulder towards small  $f$ ; the X-ray data shows some support for this (see Figures 15.60–15.63).

The mean-square “roughness” values derived from the fits also shows the increasing discrepancy towards larger values for spatial frequency. The  $\sigma^2$  evaluated for 1–10 mm<sup>-1</sup> agree much better

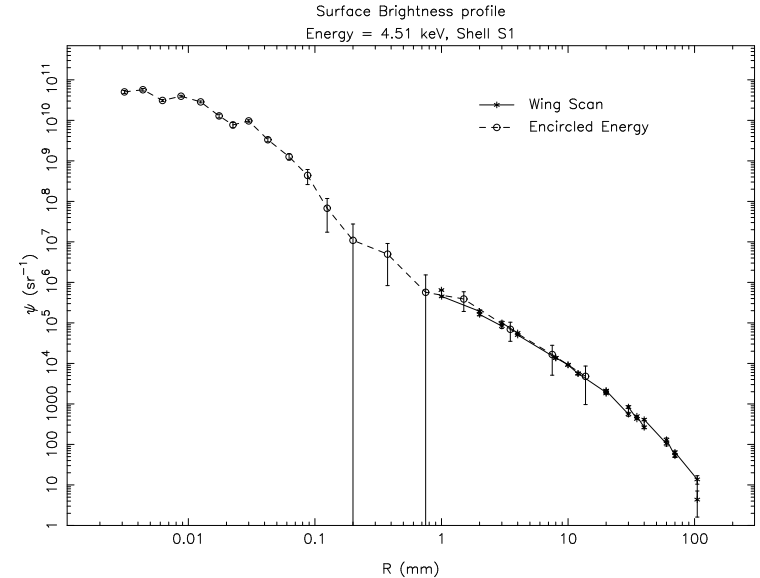


Figure 15.47: Surface Brightness vs. Radius for Shell 1S at Ti K-α. This is a composite plot based on both wing scan data and an encircled energy test.

than the values for 100–1000  $\text{mm}^{-1}$ . Comparing the values derived from the fits by integrating from 1–1000  $\text{mm}^{-1}$ , it can be seen that for shells 1 and 3, the XRCF values are about a factor of two higher than the raytrace values, about a factor of 1.7 higher for shell 4, and about 1.3 times higher for shell 6; generally, the discrepancy tends to be smaller for the smaller shells. The values for the XRCF data fits for scattering towards *vs.* away from the optic seem to be comparable except in the case of shell 3, in which case the derived roughness is considerably larger for directions away from the optic than towards the optic. As noted in the discussion of the surface brightnesses, this effect (if real, and not an artifact of the reductions and analysis) is currently not understood.

Finally, derived roughnesses from the double-quadrant scans (integrated over 1–1000  $\text{mm}^{-1}$ ) are about 3 to 3.5 times larger than the corresponding single-quadrant scans. The data were processed for the double-quadrant scans using the same value for  $a_{eff}^{tot}$  as in the single quadrant scans (see Eq. 15.1); this factor should have been a factor of two larger for the double-quadrant scans (two quadrants now contribute) so a factor of 2 of the discrepancy is explained by the normalization factor. The remaining discrepancy may be in part a result of the differences in the experimental setup (*e.g.*, the HRMA was not pitched or yawed in the double-quadrant scans), or a bias resulting from the paucity of double-quadrant data points. However, the discrepancy appears to be larger than can be easily explained by such effects.

### 15.5.1 Shell 1 scans

Table 15.11: Single quadrant wingscan  $2W_1$  fits and mean square roughness (Raytrace simulation and XRCF data, Shell 1)

| Type | Quad | Dir | a     | b     | c       | $\sigma_{1-10}^2$ | $\sigma_{10-100}^2$ | $\sigma_{100-1000}^2$ | $\sigma_{1-1000}^2$ |
|------|------|-----|-------|-------|---------|-------------------|---------------------|-----------------------|---------------------|
| sim  | 1T   | in  | 6.935 | 1.238 | 190.000 | 12.062            | 5.935               | 1.060                 | 19.056              |
| sim  | 1T   | out | 3.828 | 1.104 | 190.000 | 7.689             | 5.111               | 1.177                 | 13.978              |
| sim  | 1N   | in  | 6.914 | 1.221 | 190.000 | 12.249            | 6.269               | 1.158                 | 19.676              |
| sim  | 1N   | out | 4.612 | 1.129 | 190.000 | 9.011             | 5.663               | 1.244                 | 15.918              |
| sim  | 1B   | in  | 7.941 | 1.247 | 190.000 | 13.689            | 6.608               | 1.161                 | 21.458              |
| sim  | 1B   | out | 3.863 | 1.069 | 190.000 | 8.059             | 5.783               | 1.420                 | 15.263              |
| sim  | 1S   | in  | 7.969 | 1.247 | 190.000 | 13.738            | 6.631               | 1.165                 | 21.534              |
| sim  | 1S   | out | 3.692 | 1.068 | 190.000 | 7.711             | 5.548               | 1.366                 | 14.625              |
| xrcf | T    | in  | 6.100 | 1.009 | 761.127 | 13.830            | 12.944              | 8.396                 | 35.170              |
| xrcf | T    | out | 5.791 | 0.947 | 271.357 | 13.975            | 13.888              | 5.783                 | 33.647              |
| xrcf | N    | in  | 5.891 | 0.921 | 182.656 | 14.553            | 14.440              | 4.498                 | 33.491              |
| xrcf | N    | out | 5.350 | 0.895 | 210.773 | 13.670            | 14.729              | 5.493                 | 33.892              |
| xrcf | B    | in  | 5.824 | 1.062 | 800.000 | 12.438            | 10.335              | 6.093                 | 28.866              |
| xrcf | B    | out | 3.948 | 0.870 | 236.156 | 10.415            | 12.077              | 5.208                 | 27.700              |
| xrcf | S    | in  | 3.844 | 0.871 | 245.184 | 10.135            | 11.789              | 5.236                 | 27.160              |
| xrcf | S    | out | 7.816 | 1.041 | 314.447 | 16.965            | 13.871              | 5.347                 | 36.184              |

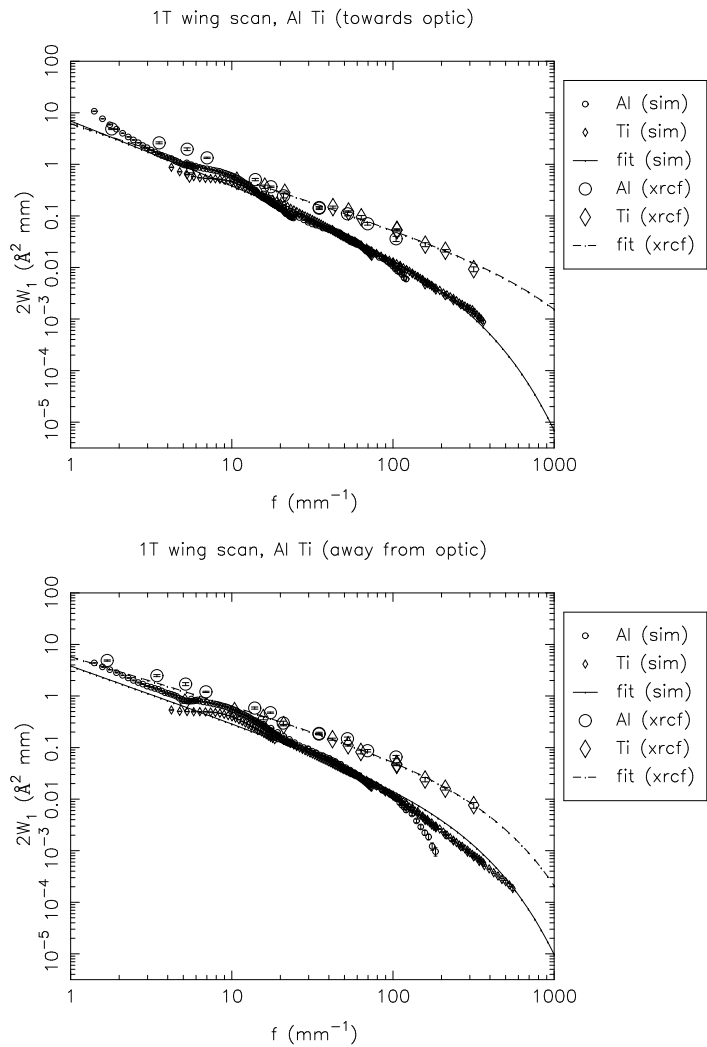


Figure 15.48: Shell 1T:  $2W_1$  profiles, towards and away from the optic. XRCF data (*xrcf*) vs. raytrace data (*sim*).

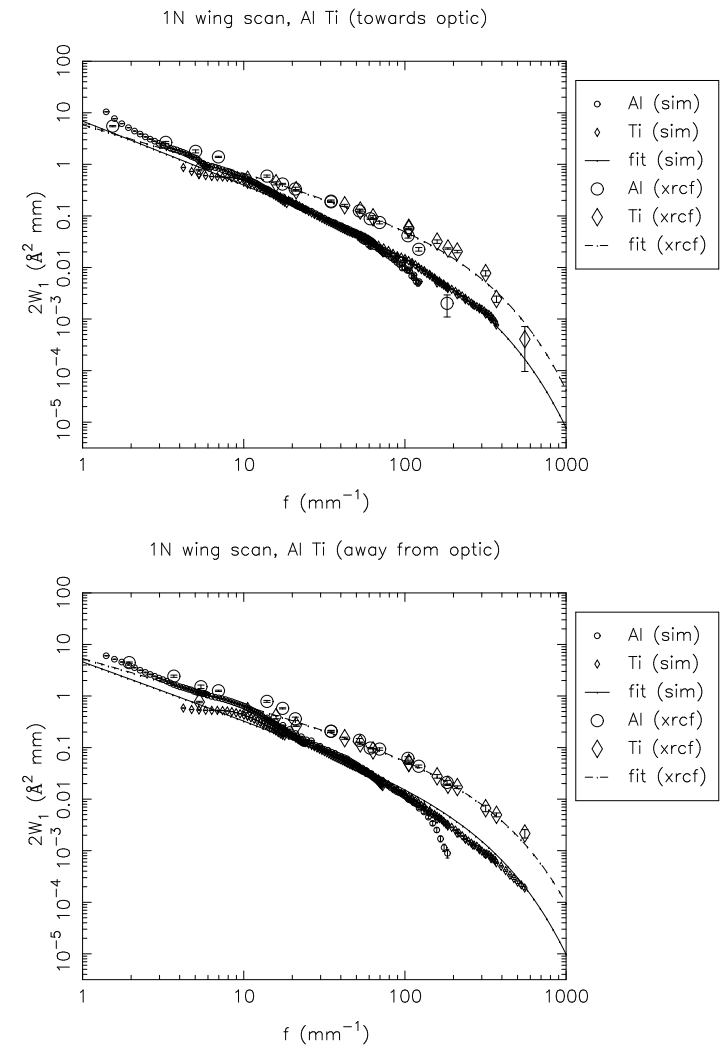


Figure 15.49: Shell 1N:  $2W_1$  profiles, towards and away from the optic. XRCF data (*xrcf*) vs. raytrace data (*sim*).

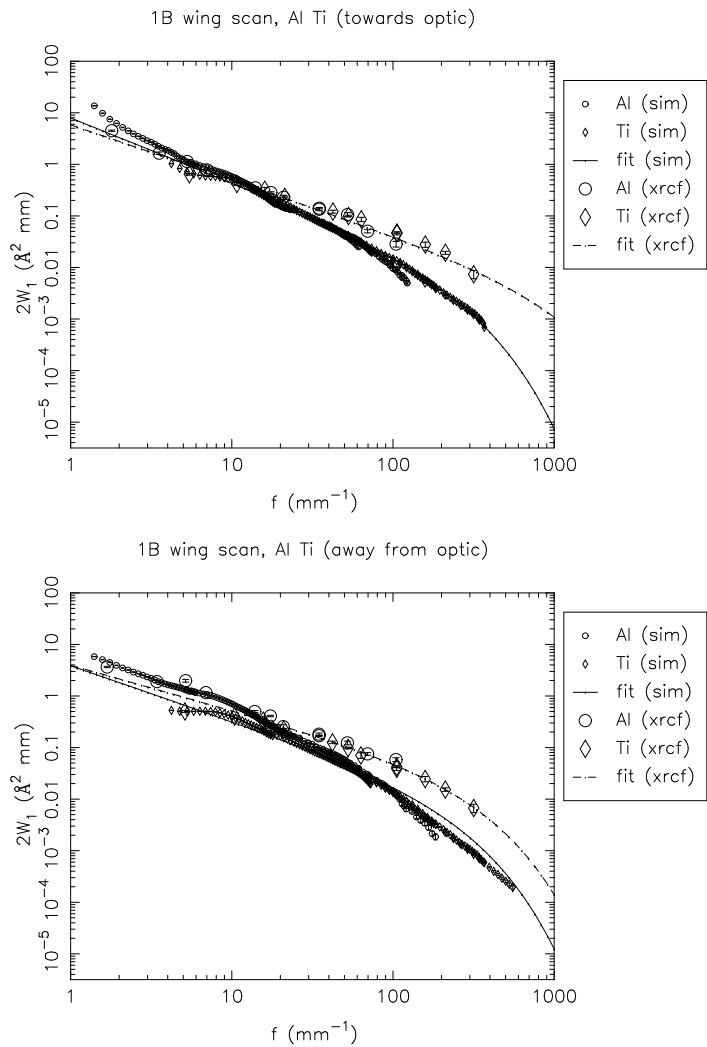


Figure 15.50: Shell 1B:  $2W_1$  profiles, towards and away from the optic. XRCF data (*xrcf*) vs. raytrace data (*sim*).

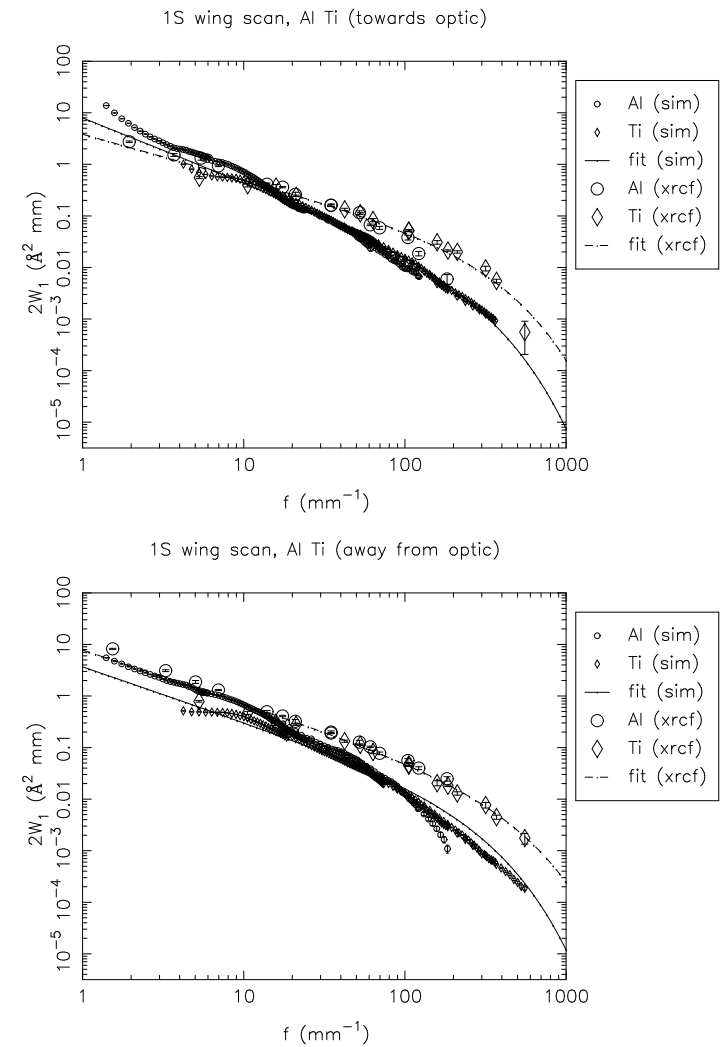


Figure 15.51: Shell 1S:  $2W_1$  profiles, towards and away from the optic. XRCF data (*xrcf*) vs. raytrace data (*sim*).

15.5.2 Shell 3 scans

Table 15.12: Single quadrant wingscan 2W<sub>1</sub> fits and mean square roughness (Raytrace simulation and XRCF data, Shell 3)

| Type  | Quad | Dir | a      | b     | c        | $\sigma_{1-10}^2$ | $\sigma_{10-100}^2$ | $\sigma_{100-1000}^2$ | $\sigma_{1-1000}^2$ |
|-------|------|-----|--------|-------|----------|-------------------|---------------------|-----------------------|---------------------|
| sim   | 3T   | in  | 3.999  | 1.555 | 2622.350 | 5.191             | 1.431               | 0.360                 | 6.982               |
| sim   | 3T   | out | 2.563  | 1.401 | 190.000  | 3.786             | 1.294               | 0.169                 | 5.250               |
| sim   | 3N   | in  | 4.831  | 1.582 | 666.650  | 6.099             | 1.533               | 0.278                 | 7.911               |
| sim   | 3N   | out | 2.729  | 1.376 | 190.000  | 4.131             | 1.493               | 0.205                 | 5.829               |
| sim   | 3B   | in  | 4.254  | 1.542 | 454.649  | 5.557             | 1.502               | 0.256                 | 7.316               |
| sim   | 3B   | out | 2.509  | 1.389 | 190.000  | 3.750             | 1.318               | 0.176                 | 5.244               |
| sim   | 3S   | in  | 3.960  | 1.508 | 210.044  | 5.296             | 1.445               | 0.166                 | 6.907               |
| sim   | 3S   | out | 2.341  | 1.400 | 190.000  | 3.462             | 1.187               | 0.155                 | 4.803               |
| <hr/> |      |     |        |       |          |                   |                     |                       |                     |
| xrcf  | T    | in  | 3.283  | 1.215 | 800.000  | 5.936             | 3.477               | 1.475                 | 10.888              |
| xrcf  | T    | out | 12.797 | 1.712 | 500.000  | 14.402            | 2.656               | 0.329                 | 17.386              |
| xrcf  | N    | in  | 2.537  | 1.138 | 360.117  | 4.954             | 3.295               | 1.142                 | 9.390               |
| xrcf  | N    | out | 12.378 | 1.609 | 488.997  | 15.230            | 3.548               | 0.542                 | 19.320              |
| xrcf  | B    | in  | 2.069  | 1.021 | 168.669  | 4.546             | 3.558               | 0.855                 | 8.959               |
| xrcf  | B    | out | 5.237  | 1.336 | 443.104  | 8.332             | 3.592               | 0.930                 | 12.854              |
| xrcf  | S    | in  | 2.243  | 1.084 | 287.982  | 4.635             | 3.407               | 1.136                 | 9.177               |
| xrcf  | S    | out | 3.704  | 1.217 | 210.807  | 6.600             | 3.460               | 0.703                 | 10.763              |

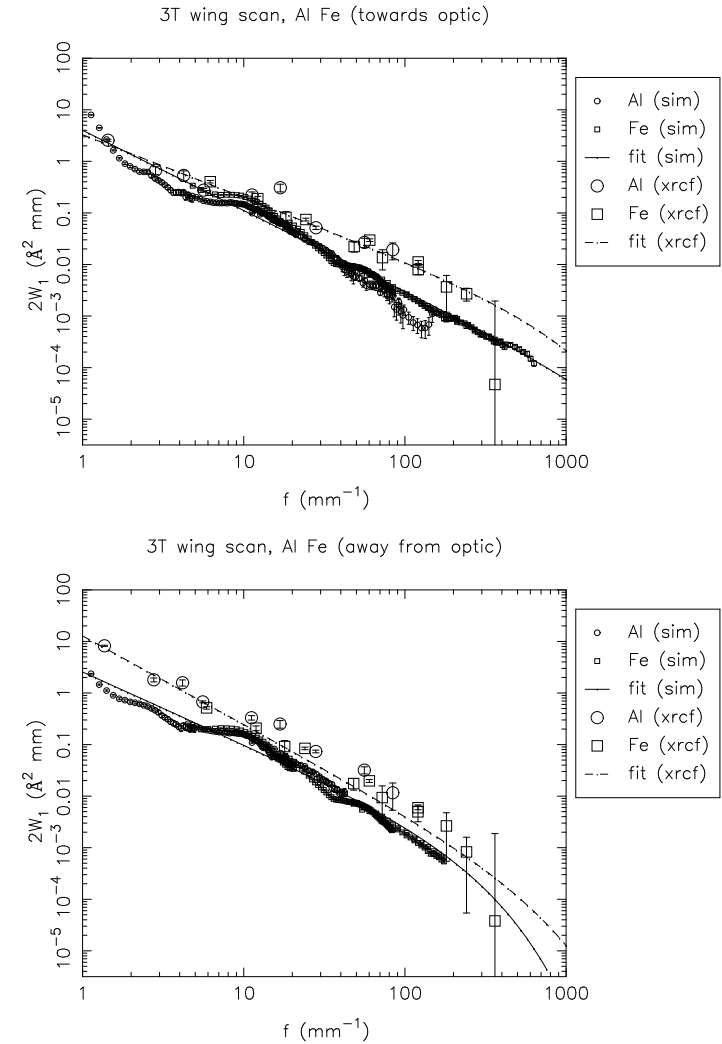


Figure 15.52: Shell 3T: 2W<sub>1</sub> profiles, towards and away from the optic. XRCF data (*xrcf*) vs. raytrace data (*sim*).

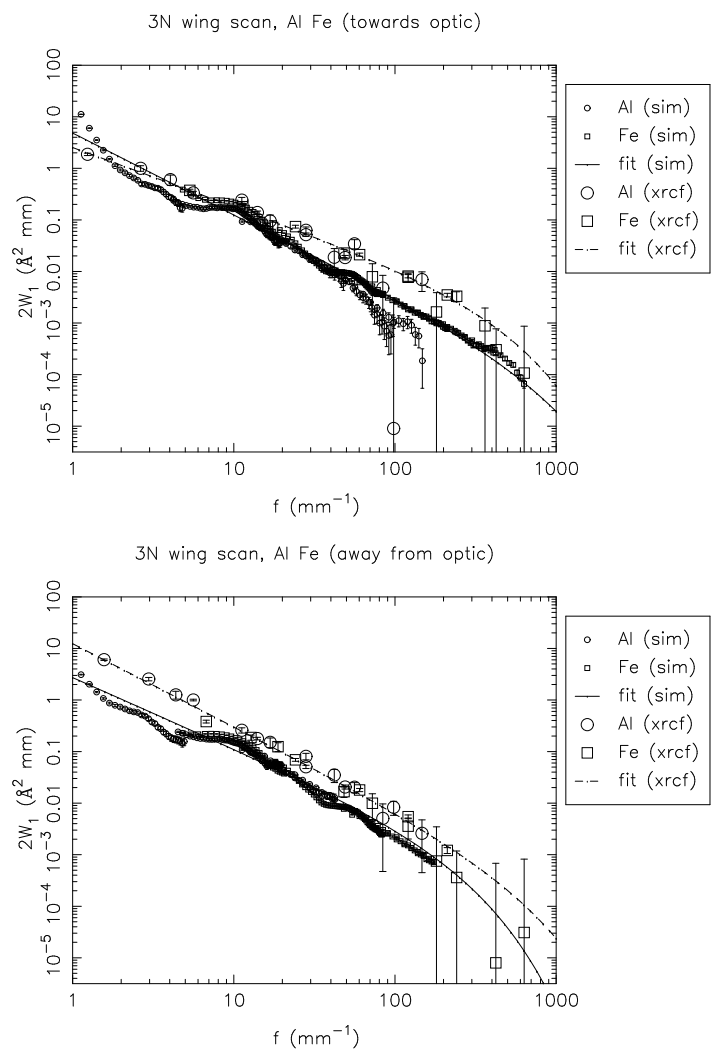


Figure 15.53: Shell 3N:  $2W_1$  profiles, towards and away from the optic. XRCF data (*xrcf*) vs. raytrace data (*sim*).

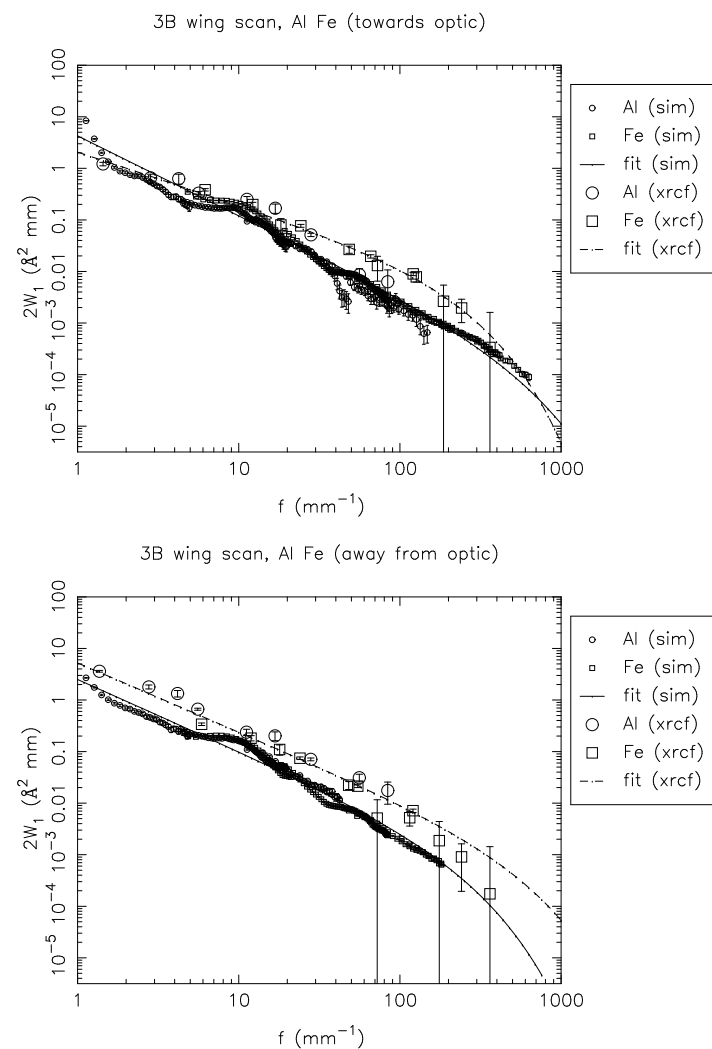


Figure 15.54: Shell 3B:  $2W_1$  profiles, towards and away from the optic. XRCF data (*xrcf*) vs. raytrace data (*sim*).

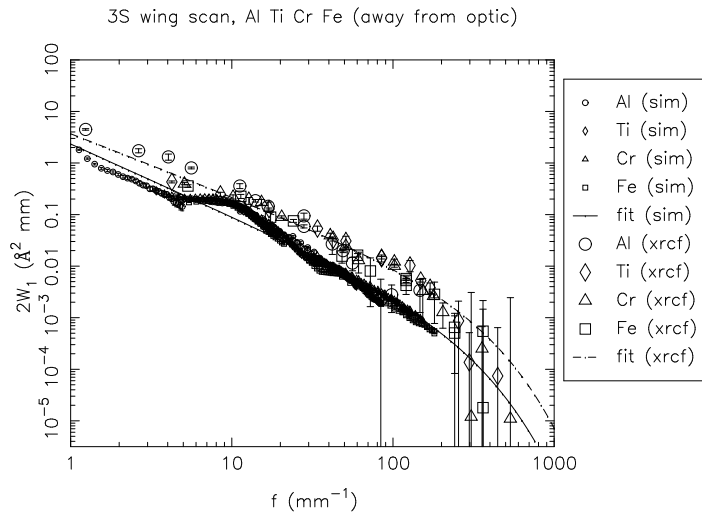
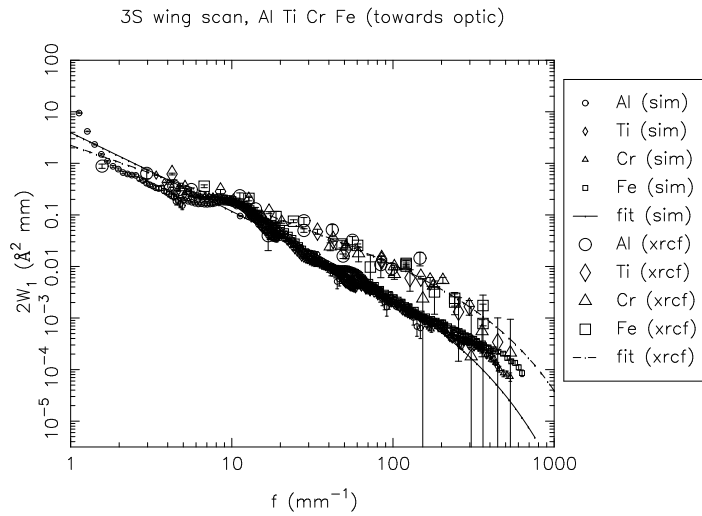


Figure 15.55: Shell 3S: 2W<sub>1</sub> profiles, towards and away from the optic. XRCF data (*xrcf*) vs. raytrace data (*sim*).

15.5.3 Shell 4 scans

Table 15.13: Single quadrant wingscan 2W<sub>1</sub> fits and mean square roughness (Raytrace simulation and XRCF data, Shell 4)

| Type | Quad | Dir | a      | b     | c         | $\sigma_{1-10}^2$ | $\sigma_{10-100}^2$ | $\sigma_{100-1000}^2$ | $\sigma_{1-1000}^2$ |
|------|------|-----|--------|-------|-----------|-------------------|---------------------|-----------------------|---------------------|
| sim  | 4T   | in  | 4.183  | 1.462 | 10000.000 | 5.929             | 2.042               | 0.685                 | 8.656               |
| sim  | 4T   | out | 3.013  | 1.363 | 346.607   | 4.657             | 1.854               | 0.398                 | 6.909               |
| sim  | 4N   | in  | 14.699 | 1.945 | 10000.000 | 13.784            | 1.560               | 0.173                 | 15.518              |
| sim  | 4N   | out | 4.619  | 1.438 | 434.562   | 6.648             | 2.268               | 0.470                 | 9.386               |
| sim  | 4B   | in  | 17.226 | 2.029 | 10000.000 | 15.176            | 1.418               | 0.130                 | 16.724              |
| sim  | 4B   | out | 3.610  | 1.384 | 337.913   | 5.466             | 2.073               | 0.421                 | 7.960               |
| sim  | 4S   | in  | 4.815  | 1.481 | 10000.000 | 6.702             | 2.208               | 0.709                 | 9.619               |
| sim  | 4S   | out | 2.768  | 1.367 | 427.547   | 4.270             | 1.713               | 0.409                 | 6.392               |
| xrcf | T    | in  | 11.518 | 1.600 | 800.000   | 14.320            | 3.478               | 0.641                 | 18.440              |
| xrcf | T    | out | 8.829  | 1.563 | 500.000   | 11.323            | 2.933               | 0.498                 | 14.754              |
| xrcf | N    | in  | 6.997  | 1.413 | 800.000   | 10.354            | 3.857               | 1.067                 | 15.278              |
| xrcf | N    | out | 7.095  | 1.358 | 500.000   | 11.053            | 4.567               | 1.195                 | 16.815              |
| xrcf | B    | in  | 20.062 | 1.791 | 800.000   | 21.185            | 3.323               | 0.404                 | 24.912              |
| xrcf | B    | out | 10.651 | 1.505 | 500.000   | 14.407            | 4.259               | 0.818                 | 19.484              |
| xrcf | S    | in  | 4.283  | 1.189 | 319.651   | 7.907             | 4.634               | 1.347                 | 13.888              |
| xrcf | S    | out | 5.439  | 1.259 | 259.463   | 9.307             | 4.557               | 1.001                 | 14.865              |

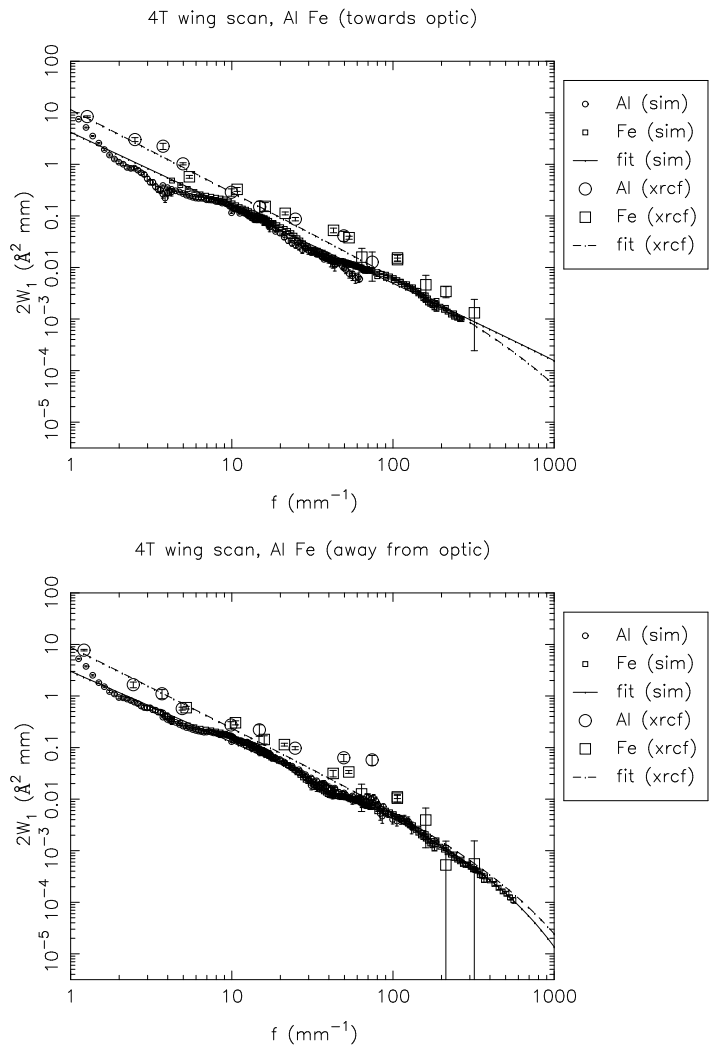


Figure 15.56: Shell 4T:  $2W_1$  profiles, towards and away from the optic. XRCF data (*xrcf*) vs. raytrace data (*sim*).

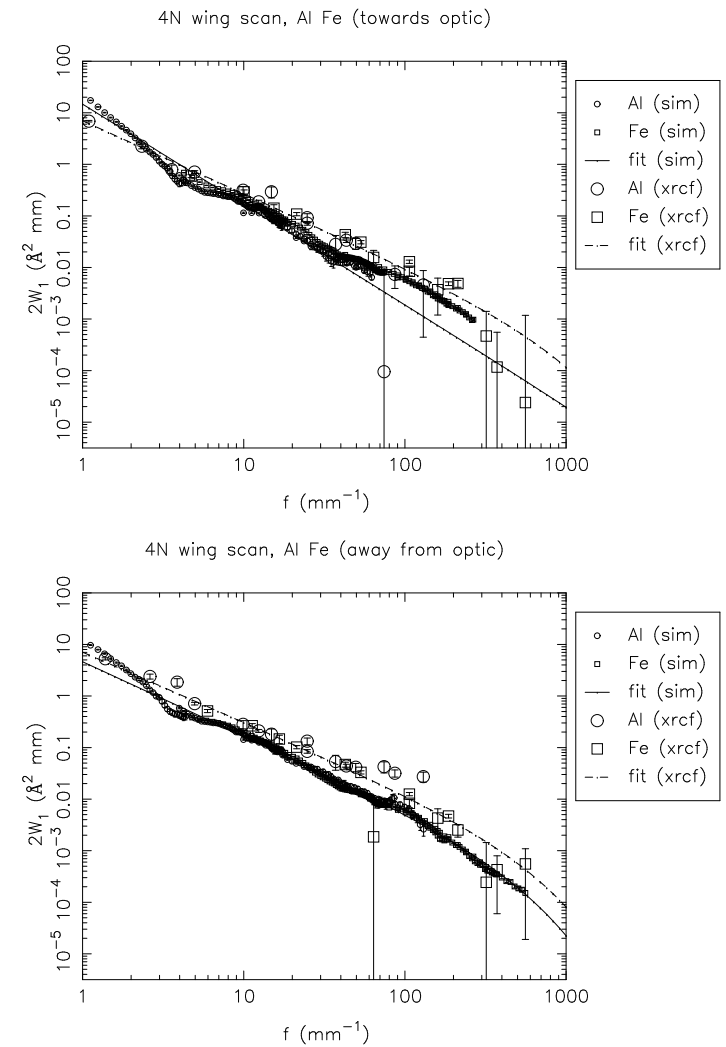


Figure 15.57: Shell 4N:  $2W_1$  profiles, towards and away from the optic. XRCF data (*xrcf*) vs. raytrace data (*sim*).

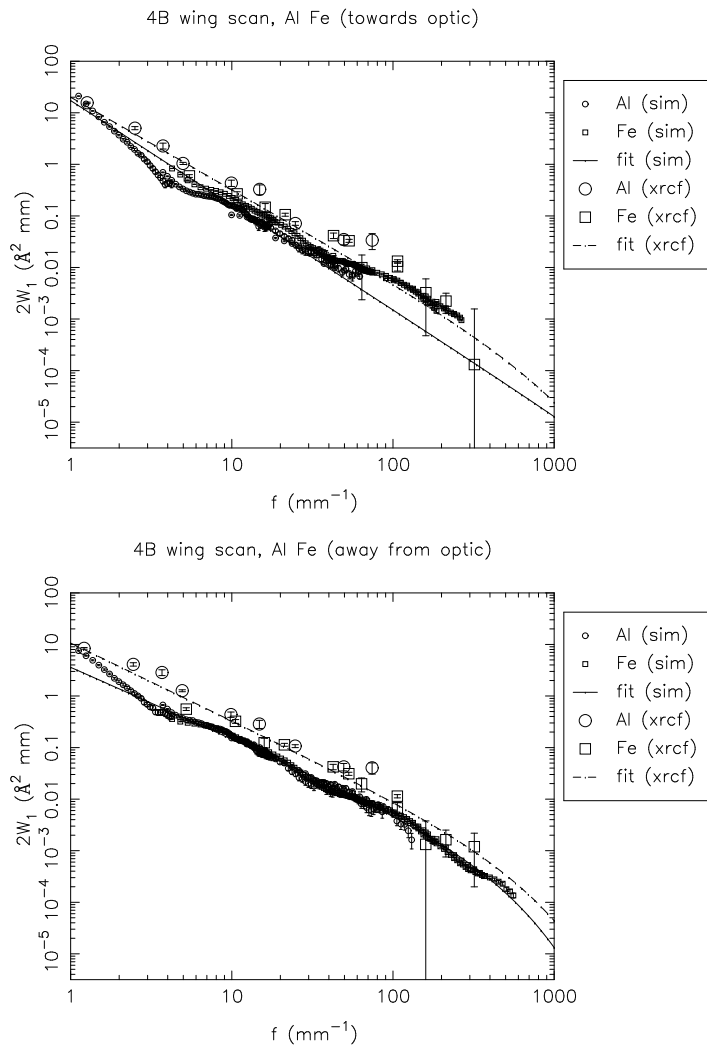


Figure 15.58: Shell 4B:  $2W_1$  profiles, towards and away from the optic. XRCF data (*xrcf*) vs. raytrace data (*sim*).

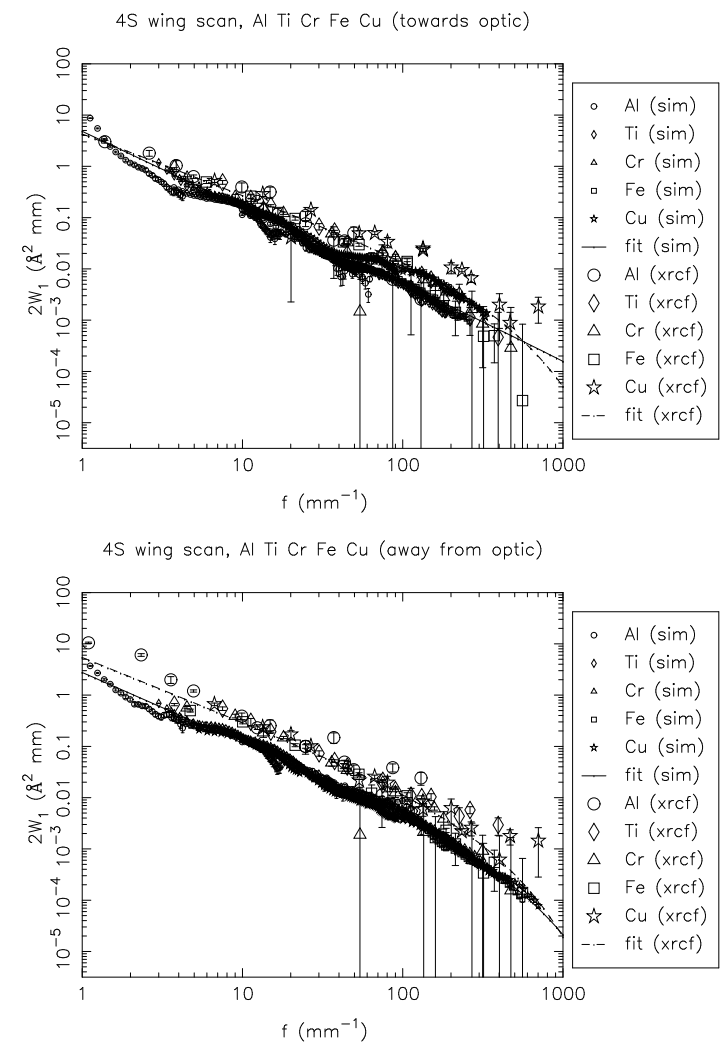
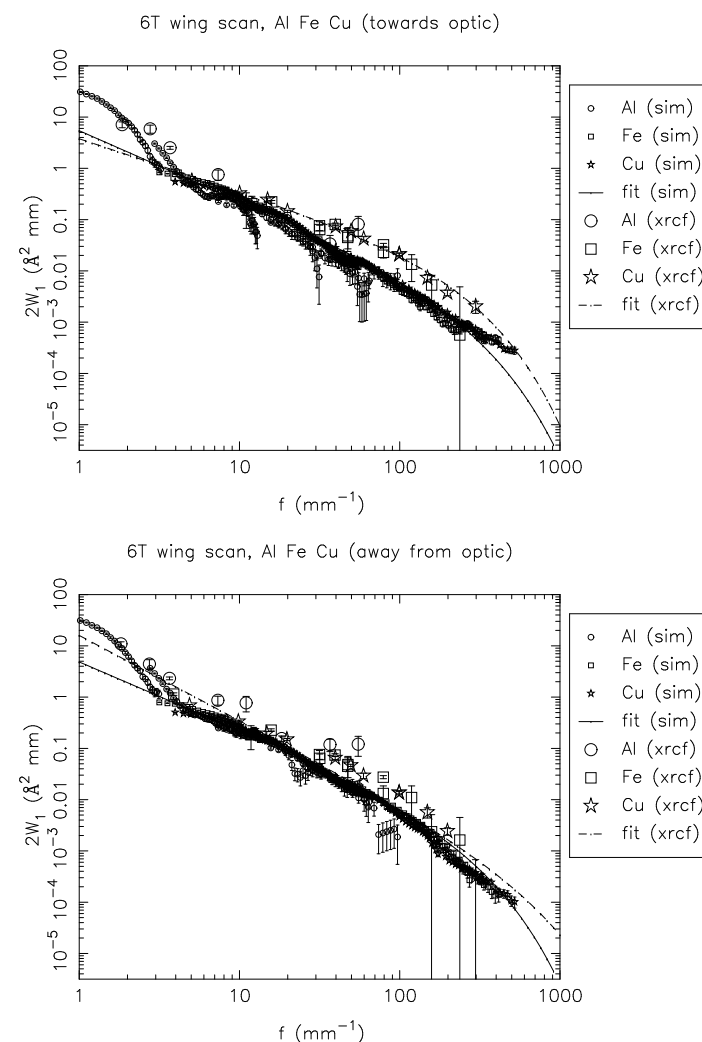


Figure 15.59: Shell 4S:  $2W_1$  profiles, towards and away from the optic. XRCF data (*xrcf*) vs. raytrace data (*sim*).

## 15.5.4 Shell 6 scans

Table 15.14: Single quadrant wingscan 2W<sub>1</sub> fits and mean square roughness (Raytrace simulation and XRCF data, Shell 6)

| Type | Quad | Dir | a      | b     | c        | $\sigma_{1-10}^2$ | $\sigma_{10-100}^2$ | $\sigma_{100-1000}^2$ | $\sigma_{1-1000}^2$ |
|------|------|-----|--------|-------|----------|-------------------|---------------------|-----------------------|---------------------|
| sim  | 6T   | in  | 5.441  | 1.365 | 190.000  | 8.323             | 3.083               | 0.432                 | 11.838              |
| sim  | 6T   | out | 4.866  | 1.334 | 190.000  | 7.680             | 3.052               | 0.454                 | 11.187              |
| sim  | 6N   | in  | 5.842  | 1.387 | 190.000  | 8.751             | 3.089               | 0.415                 | 12.254              |
| sim  | 6N   | out | 5.273  | 1.329 | 190.000  | 8.366             | 3.364               | 0.506                 | 12.236              |
| sim  | 6B   | in  | 10.047 | 1.644 | 1523.130 | 12.037            | 2.685               | 0.516                 | 15.238              |
| sim  | 6B   | out | 4.877  | 1.334 | 190.000  | 7.697             | 3.059               | 0.455                 | 11.211              |
| sim  | 6S   | in  | 6.953  | 1.456 | 190.734  | 9.743             | 2.946               | 0.347                 | 13.036              |
| sim  | 6S   | out | 4.869  | 1.343 | 190.000  | 7.617             | 2.968               | 0.434                 | 11.019              |
| xrcf | T    | in  | 3.785  | 1.027 | 172.717  | 8.264             | 6.412               | 1.558                 | 16.233              |
| xrcf | T    | out | 15.978 | 1.658 | 500.000  | 18.834            | 3.929               | 0.545                 | 23.308              |
| xrcf | N    | in  | 4.932  | 1.081 | 107.681  | 10.005            | 6.201               | 0.810                 | 17.017              |
| xrcf | N    | out | 6.979  | 1.232 | 153.534  | 12.167            | 5.858               | 0.868                 | 18.893              |
| xrcf | B    | in  | 28.228 | 2.147 | 800.000  | 22.787            | 1.581               | 0.088                 | 24.456              |
| xrcf | B    | out | 6.293  | 1.208 | 194.071  | 11.304            | 5.973               | 1.151                 | 18.428              |
| xrcf | S    | in  | 4.812  | 1.089 | 135.492  | 9.745             | 6.277               | 1.061                 | 17.084              |
| xrcf | S    | out | 6.796  | 1.225 | 120.423  | 11.859            | 5.514               | 0.637                 | 18.010              |

Figure 15.60: Shell 6T: 2W<sub>1</sub> profiles, towards and away from the optic. XRCF data (*xrcf*) vs. raytrace data (*sim*).

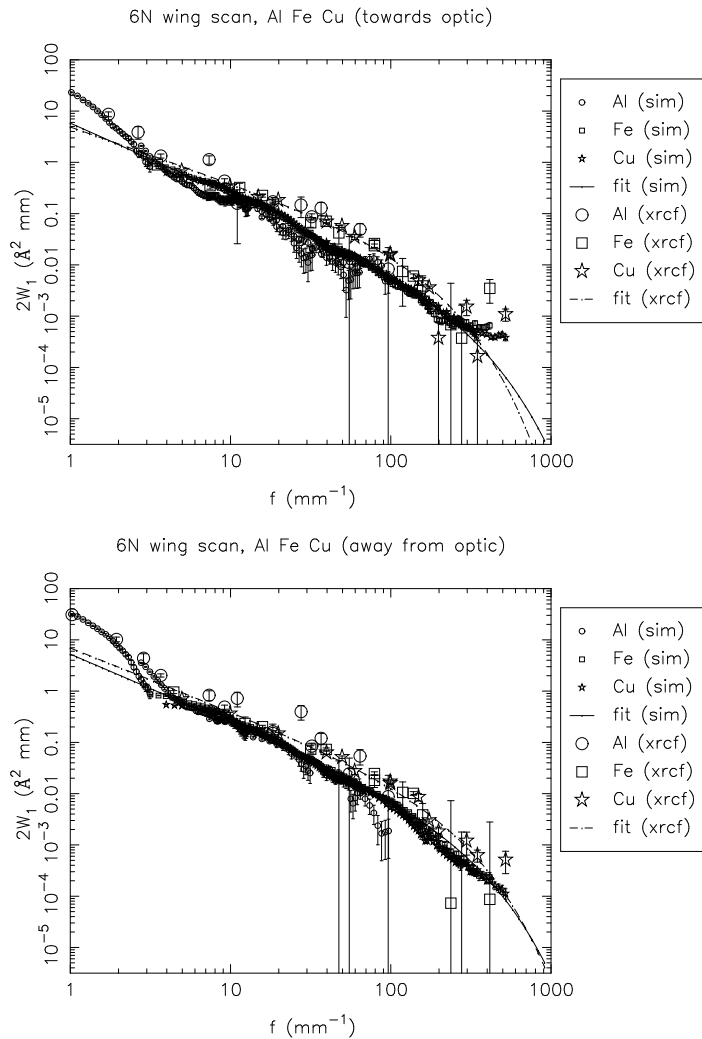


Figure 15.61: Shell 6N:  $2W_1$  profiles, towards and away from the optic. XRCF data (*xrcf*) vs. raytrace data (*sim*).

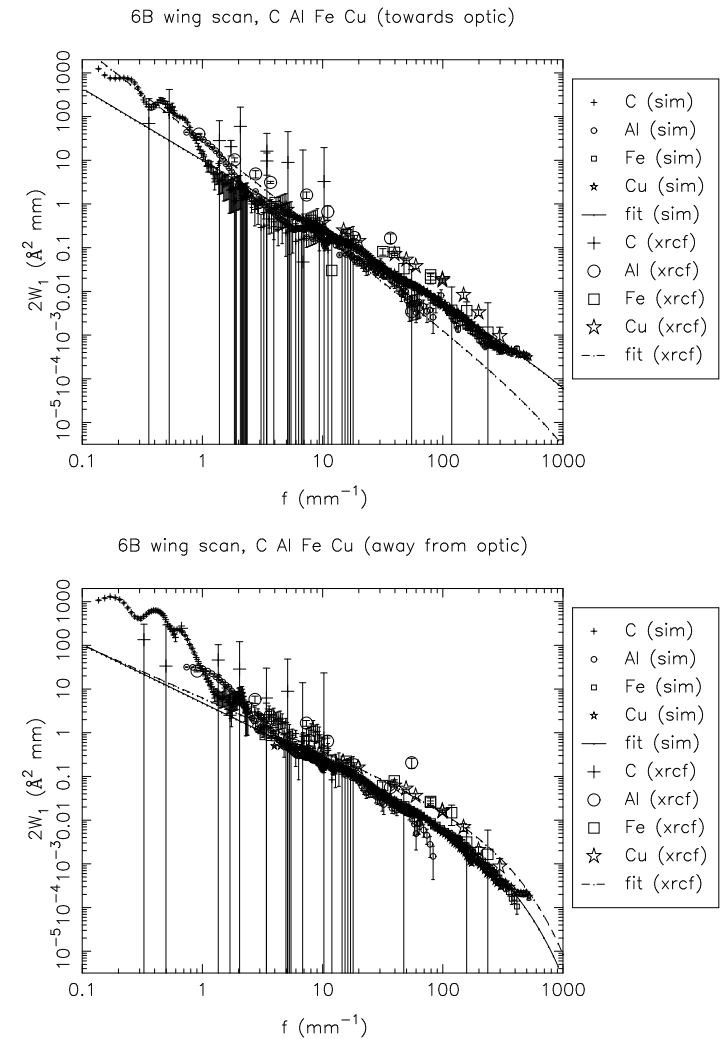


Figure 15.62: Shell 6B:  $2W_1$  profiles, towards and away from the optic. XRCF data (*xrcf*) vs. raytrace data (*sim*).

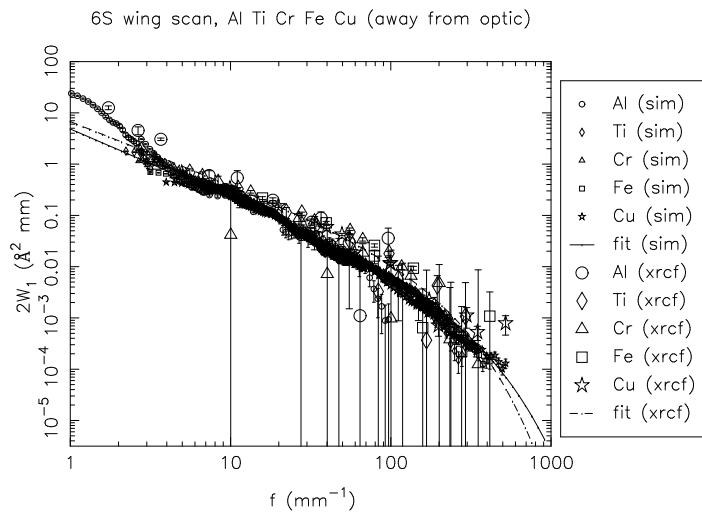
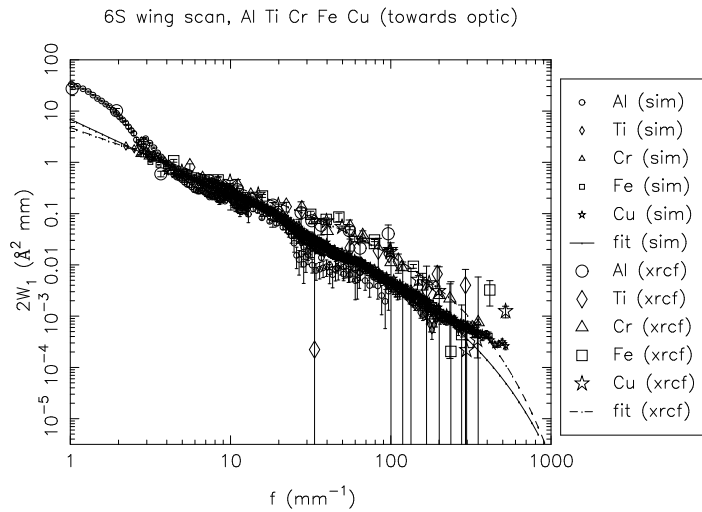


Figure 15.63: Shell 6S: 2W<sub>1</sub> profiles, towards and away from the optic. XRCF data (*xrcf*) vs. raytrace data (*sim*).

### 15.5.5 2 Quadrant Scans

Table 15.15: Double quadrant wingscan 2W<sub>1</sub> fits and mean square roughness (Raytrace simulation and XRCF data, Shell 4NS)

| Type | Quad | Dir  | a      | b     | c        | $\sigma_{1-10}^2$ | $\sigma_{10-100}^2$ | $\sigma_{100-1000}^2$ | $\sigma_{1-1000}^2$ |
|------|------|------|--------|-------|----------|-------------------|---------------------|-----------------------|---------------------|
| sim  | 4NS  | both | 40.548 | 2.293 | 1000.000 | 29.687            | 1.480               | 0.062                 | 31.230              |
| xrcf | NS   | both | 38.249 | 1.763 | 800.000  | 41.332            | 6.912               | 0.893                 | 49.138              |

Table 15.16: Double quadrant wingscan 2W<sub>1</sub> fits and mean square roughness (Raytrace simulation and XRCF data, Shell 6NS)

| Type | Quad | Dir  | a      | b     | c        | $\sigma_{1-10}^2$ | $\sigma_{10-100}^2$ | $\sigma_{100-1000}^2$ | $\sigma_{1-1000}^2$ |
|------|------|------|--------|-------|----------|-------------------|---------------------|-----------------------|---------------------|
| sim  | 6NS  | both | 49.306 | 2.280 | 1000.000 | 36.424            | 1.874               | 0.081                 | 38.379              |
| xrcf | NS   | both | 32.181 | 1.500 | 200.000  | 43.321            | 11.952              | 1.343                 | 56.616              |

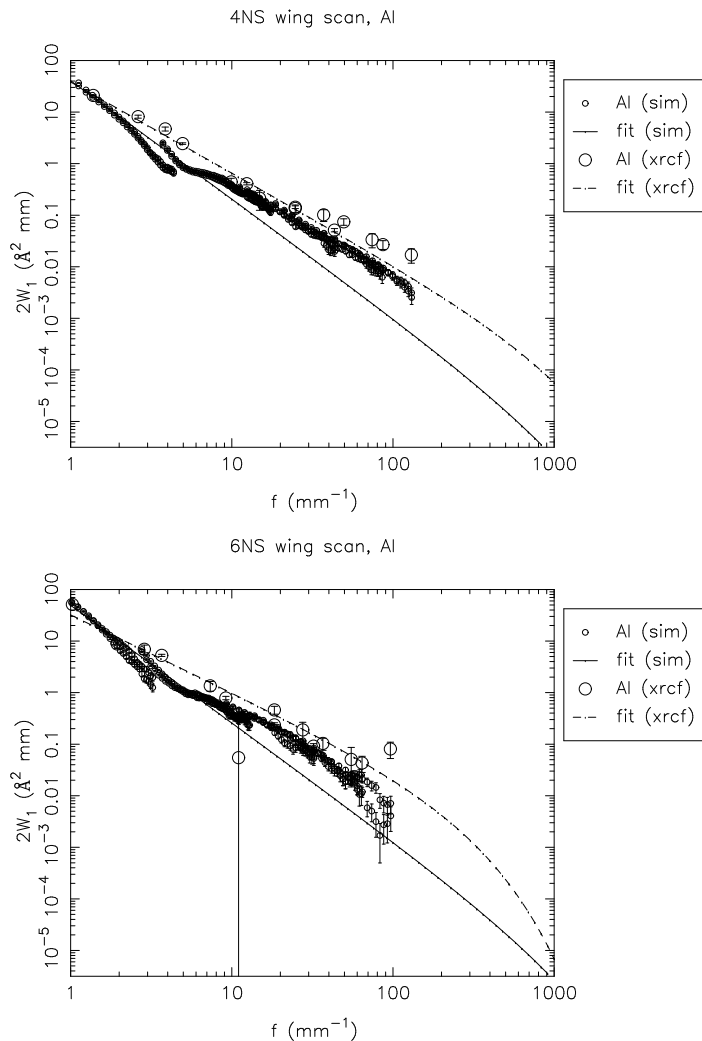


Figure 15.64: Double quadrant wing scans. Top: Shell 4 N and S quadrants:  $2W_1$  profiles. Bottom: Shell 4 N and S quadrants:  $2W_1$  profiles. XRCF data (*xrcf*) vs. raytrace data (*sim*).

## 15.6 Outstanding Analysis Issues

The analysis can be improved in a number of ways:

- In the case of the raytrace simulations, the fits to the surface brightness data and to the  $2W_1$  data are not very good in many cases. The raytrace data show structure which is not captured by the simple fit function; on the other hand, the XRCF data set is sparse enough that a more elaborate fitting function is not really justified. In the raytrace fits, a lower limit to the exponential cutoff scale was specified. This was estimated by inspecting the resulting fits; the same cutoff value was used for all of the  $\psi$  fits (and similarly, for the  $2W_1$  fits). Consequently, the fit at large radius can be bad. This affects the estimates of the fractional effective area outside the 35 mm pinhole (in the case of the  $\psi$  fits) or the mean square roughness  $\sigma^2$  (in the case of the  $2W_1$  fits).
- The truncation of the raytrace data sets to remove points affected by shutter vignetting was done by estimating a cutoff based on visual inspection of the curves. Raytraces with/without adjacent shutters in (shutters for other shells in the same quadrant) would provide a better handle on when the shutter vignetting kicks in.
- The surface brightness,  $\psi$ , is scaled by a factor  $2 \times 88/360$  to account for the fact that the experiment used a single quadrant at a time. This should be checked against raytraces for 1 vs. 4 quadrants open in a given direction, *e.g.*, nS vs. 1S3S4S6S, and for on-axis versus tilted HRMA cases. However, such raytraces would have to be much longer than the ones used in the current analysis. For now, this effect should more or less scale out because the raytraces were processed in the same way as the XRCF data.
- The comparison of scattering towards vs. away from the optic has only been given a cursory examination; further work needs to be done to determine whether there are discernible trends from quadrant to quadrant.
- The transverse wing scan data poorly understood at present. They are significantly below the corresponding in-plane measurements, but they need to be compared to raytraces in order to assess whether they are consistent with the scattering calculations.
- The double-quadrant wing scan data are *very* sparse; the analysis and interpretation of these data are incomplete at present.

## 15.7 Implications for Scattering Models

From the foregoing it is clear the raytrace scattering model needs to be improved. The raytraces consistently underpredict the pinhole effective area for the larger pinholes. The surface brightness plots and the  $2W_1$  plots indicate a steeper power-law slope than is seen in the wing scan data. The mean-square roughness for spatial frequencies 1 – 1000  $\text{mm}^{-1}$  as deduced from the XRCF wing scan data are larger than that from the raytrace by about a factor of two for shells 1, 3, and 4, and about a factor 1.3 for shell 6. The disagreement between X-ray determinations and raytrace estimates get worse for larger spatial frequency  $f$ ; this can also be seen in the figures in that the slopes of the  $2W_1$  curves based on XRCF data tend to be flatter than the  $2W_1$  curves obtained from the raytraces. The derived roughness parameter,  $\sigma^2$ , obtained by integrating the  $2W_1$  functions over some passband, show puzzling variations: in quadrants 1S, 3T, 3N, 3B, 3S, and 4S, the  $\sigma^2$  derived from the fits for scattering away from the optic surface are considerably larger than those for scattering towards the optic surface. In addition, the roughness derived from the double-quadrant scans is a factor of about 2 larger than that obtained from the single quadrant scans (taking into account the difference in normalization); this may result in part from the different illumination

pattern (tilted *vs.* untilted HRMA), but further investigation is warranted.